CREATING COLLAGEN 3D MICROENVIRONMENT BY DEVELOPING PNEUMATIC ACTUATED SOFT MICROMOLD (PASMO) FOR BIOLOGICAL APPLICATION

A Dissertation

by

PO-JUNG HUANG

Submitted to the Office of Graduate and Professional Studies of
Texas A&M University
In partial fulfillment of the requirements for the degree of

DOCTOR OF PHILOSOPHY

Chair of Committee,	Jun Kameoka
Committee Members,	Hong Liang
	Haiyan Wang
	Sungyon Lee
	Pao-Tai Lin
Head of Department,	Ibrahim Karaman

December 2017

Major Subject: Materials Science and Engineering

ABSTRACT

Small volume, high surface area and protective fibulas scaffold of collagen modular microenvironment improves cell viability and proliferation. Therefore, the ability to produce collagen modular microenvironment accurately and reliably is of most importance to the advancement of tissue engineering. Currently, no such fabrication technique exists due to the inherent fragility of collagen. Herein, we report the very first platform that addresses such challenges. Pneumatic actuated soft micro mold (PASMO) composes asymmetric structure, which performs different mechanical properties. PASMO device is classified as particles' template(top layer), air channel layer(middle layer) and resistance(bottom layer). The major deformation of PASMO is assigned to particles' template layer because the mechanical property of particles' template is less than resistance layer. Therefore, the deformation would form on particles' template to expand and extract microparticles from PASMO device after increasing inner pressure. Soft micro mold with pneumatic extraction actuator not only can produce arbitrary shapes of collagen microstructures precisely but also can encapsulate cells inside without causing damage during the extraction process.

MDA-MB-231-GFP encapsulated in collagen microcubes can fully stretch and survive well. Moreover, MDA-MB-231-GFP in collagen microcubes can sense the treatment of Paclitaxel and the size of microcubes changed as following the different concentration of Paclitaxel due to the inhibition of cellar division. Furthermore, creating cancer microenvironment can efficiently localize cancer cells at the specific location so that it minimizes the varieties of experiments.

Another application is for cell therapy, like beta cells encapsulation for creating artificial islet. Artificial islets are micro-disk can secrete insulin based on the stimulation of glucose from the surrounding. Blood vessels can successfully form around the implanted artificial islets. This formation of the blood vessel for subcutaneous transplantation not only can regulate the level of glucose in blood but also can simplify surgery to avoid the risk. For multiple locations of implanted artificial islets clusters, blood vessels can also form connections between these two groups.

DEDICATION

This dissertation is lovingly dedicated to my family.

ACKNOWLEDGEMENTS

I would like to thank my advisor, Dr. Jun Kameoka for his unrelenting guidance and support throughout my research. I would also like to thank my committee members, Dr. Liang, Dr. Wang, Dr. Lee, and Dr. Lin, for their valuable insights and suggestion on my research.

The work of xenograft is in collaboration with Dr. Chao-Kai Chou, and Dr. Mien-Chie Hung at the Department of Molecular and Cellular Oncology, MD Anderson Cancer Center. The work of generating artificial islet is in collaboration with Dr. Pradip Saha at Molecules and Cell Biology, Baylor College of Medicine. The simulation work is in partnership with Jian Qu and Dr. Anastasia Muliana at the Department of Mechanical Engineering, Texas A&M University.

Thanks also go to my friends and colleagues and the department faculty and staff for making my time at Texas A&M University a great experience. I also want to extend my gratitude to the team at Aggiefab and Material Characterization Facility at Texas A&M University.

Last but not least, I want to thank my parents and brother for their encouragement and to Yi-Hsuan for her patience and love. Without you, this could not be possible.

CONTRIBUTOR AND FUNDING SOURCES

Contributor

This work was supervised by a dissertation committee consisting of Professor Jun Kameoka and Hong Liang, Haiyan Wang, Pao-Tai Lin of the Department of Materials Science and Engineering and Professor Sungyon Lee of the Department of Mechanical Engineering.

All work for the dissertation was completed by the student, under the advisement of Jun Kameoka of the Department of Materials Science and Engineering.

Funding Sources

There are no outside funding contributions to acknowledge related to the research and compilation of this document.

NOMENCLATURE

2D	two-dimensional
3D	three-dimensional
ECM	extracellular matrix
HA	hyaluronic acid
PEG	poly(ethylene) glycol
PEGDA	poly(ethylene) glycol diacylate
RGD	arginylglycylaspartic acid
DNA	deoxyribonucleic acid
UV	ultraviolet
Gly	Glycine
Pro	Proline
Lys	Lysine
Asp	Aspartic acid
Hyp	Hydroxyproline
FAK	focal adhesion kinase
EMT	epithelial–mesenchymal transition
PASMO	pneumatic actuated soft micromold
cPASMO	circular pneumatic actuated soft micromold
SHG	secondary harmonic generation
GFP	green fluorescent protein
MDR	multidrug resistance derived

MCF-7	Human Breast Cancer Cell Line
T4-2	Human Breast Cancer Cell Line
MDA-MB-231	Breast Cancer Cell Line
U2OS	Osteosarcoma Cell Line
HMT-3522	Mutated from normal cell line
DMEM	Dulbecco’s Minimal Essential Medium
FBS	Fetal bovine serum
AsPC1-Luc	Pancreatic cells line expressed luciferase
BMP4	Bone morphogenetic protein 4
FGF	Fibroblast Growth Factor
EGFR	Epidermal growth factor receptor
IBMIR	instant blood-mediated inflammatory reaction

TABLE OF CONTENTS

LIST OF FIGURES

LIST OF TABLES

1. INTRODUCTION- 3D MICROENVIRONMENT*

1.1 2D and 3D Cell Culture

In vivo study is the method to simulate the human response under different stimuli from different treatment, especially for drug screening.[1,2] However, in vivo study hinders the screening rate of drug development because of time-consuming process. Time-consuming process comes not only from complicated metabolic processes of living organism but also from discovering and isolating the meaningfully biological information from individual variability. *In vitro* study is developed as a crucial tool to speed up and simplify the screening process for realizing biological functions under different stimuli. *In vitro* study started from 1950s, and it stands for culturing microorganism, cells, or biological molecular outside their normal biological surrounding. In 1970s, NCI funded study evaluated the technique, which develops colony assay to grow fresh human patient cells in soft agar for drug screening.[3] They re-tested over 79 compounds of anticancer drugs, which are inactive in the *in vivo* drug screening, especially for breast, colorectal, kidney, lung, melanoma, and ovarian. However, soft agar assays has limitation for plating efficiency because of lacking of constant supply of fresh patient samples, even the efficiency is 70-80%. As a result, this assay is still considered as impractical drug screening tool.[4] To improve screening efficiency, cancer research relies on two-dimensional cell cultures (2D culture).[5,6] 2D culture is the process that we culture cell on petri dish or culture flask. Cancer cell line is isolated from patients as source and these cells are transferred on petri dish, which

* Reprinted with permission from SOFT ROBOTICS, Year 2017, published by Mary Ann Liebert, Inc., New Rochelle, NY

contains culture media as nutrient. In particular, cells are attached onto rigid and flat substrates, which force them to polarize and increase their exchange area for culturing. However, the biological function in 2D culture model is eliminated due to abnormal morphology of cells.[7,8] Abnormal cell morphology can influence many cellular process including cell proliferation, differentiation, apoptosis, and gene and protein expression.[9] A variety of cell lines indicates that cell proliferation rate is significantly different in 2D and 3D culture.[10-15] For example, osteosarcoma cell line U2OS or breast adenocarcinoma cell line MCF-7 in 3D type I collagen microenvironment have reduced proliferation rate compare to 2D culture model.[12] The main reason is that transcriptional and translational levels are changed. When cells are isolated out of their natural microenvironment, the cells would adopt the new microenvironment by their biological functions. The obvious cellular function is cell growth and proliferation. Approximately 30% of genes are differently expressed in 2D culture, especially interfering cell proliferation. This support the observation of cell proliferation in 2D culture is faster than in 3D culture.[16] Moreover, the signal transduction pathway would also be interrupted and then the differentiation and apoptosis would be influenced. For example, tenascin C can regulate FGF2 and BMP4 signaling pathway, both which are related with the differentiation of neural stem cells.[17] These two pathway cannot be observed and monitored in 2D culture because of lacking of cell-cell or cell-matrix interaction.[18] Eventually, 2D culture is not a proper way to use as a tool for further biological application. A variety of researches presents that 2D culture would mislead the sensitivity of drugs.[19] In one study, human breast cancer cell line (T4-2) isolated and mutated from normal cell line (HMT-3522) cultured

in 3D collagen model. The epidermal growth factor receptor (EGFR) antibody were treated with encapsulated T4-2 and the down-regulation between EGFR and β1-integrin can be observed. On the other hand, down-regulation between EGFR and β1-integrin in 2D culture cannot be distinguished after treating EGFR antibody because of no cell-cell interaction.[19] Another misleading of bio-function in 2D culture is multidrug resistance. A human breast cancer cell line (MCF-7) and its multidrug resistance derived cell line (MDR-MCF-7) were cultured in 2D and 3D microenvironment, respectively. Both types of cancer cells were reduced the proliferation after treating anti-cancer drug doxorubicin either in 3D culture or in 2D culture. However, MCF-7 reduced the sensitivity of doxorubicin in 3D culture and MDR-MCF-7 presented no response to anti-drug treatment. The main reason is that 2D culture is the monolayer culture, which can expose large area to sense the surrounding stimuli and eliminate the physical barrier. As a result, the sensitivity of drug or surrounding stimuli in 2D culture is more sensitive than in 3D culture.[20-22] Figure 1 shows the relationship of biological function in 2D and 3D culture.

1.2 3D Cell Culture

The conventional 2D cell culture is used to help us realize the complex cellular physiology, like how cells have responds to surrounding stimuli. While 3D cell culture is designed as a tool to mimic *in vivo* condition. Figure 2 is the schematic diagram of 3D cell culture. 3D cell culture is to encapsulate cells in extracellular matrix (ECM) within 3D structure instead of 2D monolayer cell sheet. The target cells are mixed and encapsulated in ECM, which contains porous structure. oxygen, nutrient, or surrounding stimuli is allowed to diffuse into 3D microenvironment through porous structure. After metabolism, the product or waste can also diffuse out of microcapsule. 3D microenvironment can be used as a microcapsule to implant it into animal for monitoring the biological function in animal model because ECM plays a crucial role to resist of attacking from immune cells. Therefore, the immunoresponse can be eliminated and the immunosuppressant is not necessary to apply in animal experiment. Some immunosuppressant would affect the cell function and even lose biological function. For example, cyclosporine can effectively inhibit the immunoresponse, however, cyclosporine is highly toxic for liver, kidney, and pancreatic beta cells. As a result, there are more irregular biological response would be observed in order to mislead the cellular function.[23]

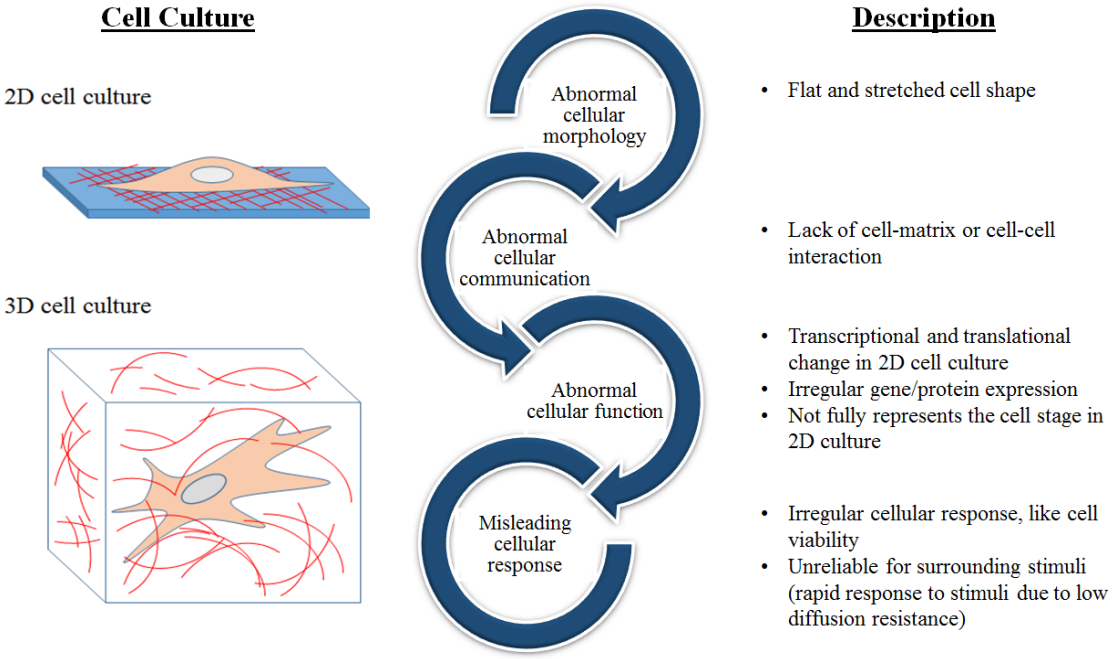

Figure 1 Comparison between 2D and 3D cell culture. 2D cell culture presents abnormal cell morphology and lacks of cell-cell or cell-matrix interaction so that the cellular function would be interfered

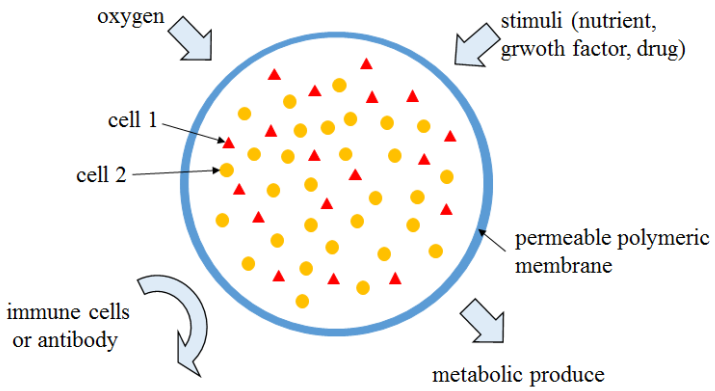

Figure 2 Schematic diagram for 3D microenvironment. Oxygen and nutrient can be allowed to diffuse inside the 3D microenvironment. While, the metabolic waste can also diffuse out due to porous structure. Moreover, microenvironment is also a good barrier for immune cells to reduce the immune response

1.3 Hydrogel Material

The properties of extracellular matrix play important roles for biologic function because it would generate different cell-cell or cell-matrix interaction. Then, the signal transduction pathway would be triggered as different pathway based on cell-matrix interaction.[24] In cancer research, the mechanical properties of ECM would activate different progression of cancer development. For example, stiffer matrix can enhance cell growth, focal adhesion, integrin clustering and matrix invasion. Cells are able to sense the matrix stiffness and activate the mechanical signal transduction pathway, which is known as mechano-transduction. This pathway has been influenced cell proliferation and differentiation.[25-27]

Polymeric hydrogels are composed by hydrophilic and porous structure, which can easily to allow water, oxygen, and nutrient to diffuse and exchange in this network. Hydrophilic network is composed by controlling physical or chemical condition to make cross-linking reaction. Therefore, the physical or chemical properties of polymeric hydrogel, like mechanical properties, swelling ratio, degradation rate, 3D architecture, and bioactivity, can be adjusted easily by the level of cross-linking.

Polymeric hydrogels can be classified as natural and synthetic hydrogel. Natural hydrogel, like collagen,[28] hyaluronic acid (HA),[29] alginate,[10] chitosan,[30] silk fibrils,[31] agarose,[32]and cellulose,[33] is isolated from organism. Since these materials are extracted from natural source, they have excellent biocompatibility, bioactivity and biodegradability, and low immunogenicity for artificial ECM. However, they still have some disadvantages for cell encapsulation. For example, alginate has good bioactivity

for cell viability, but alginate cannot be used as cell microcapsules because of inflammatory response. Otterlei et al. found that alginate microcapsule would induce and active the human monocytes and then trigger inflammatory response when the accumulation of monocytes is formed.[34-35] Moreover, Soon-Shiong et al. also noticed that the cell morphology in alginate is abnormal growth.[36] Chokkalingam et al. used agarose to encapsulate and immobilize cell in microcapsule. The immunoresponse is not much obvious than alginate but the solidification of agarose needs to heat up for melting then mixed with cells for encapsulation. The process is hard to control and the reproducibility for encapsulating is lower than other material. Moreover, increasing temperature sometimes kills cells because the operating temperature is over the tolerance for cells.[32] Another disadvantage for natural ECM is weak mechanical properties. Tan et al. used chitosan as the target material for cell encapsulation. The structure of chitosan microcapsule is soft and unstable. Therefore, chitosan need to mix with collagen to stabilize the structure and improve the mechanical properties.[37]

To overcome these shortcoming of natural ECM, researchers develop synthetic polymer as the material of ECM due to their flexible chemistry and biophysical properties. The quality of synthetic polymer is consistency because the batch-to-batch process is easy to control and reproduce. Poly(ethylene glycol) (PEG)-based hydrogel is an outstanding example for synthetic hydrogel. PEG not only has excellent mechanical property but also has well-tuned structure through modifying chemical composition. Moreover, microfluidic system and photolithography process can be integrated into producing PEG hydrogel for mass production.[38] Moreover, bioinert is also the signature

property for synthetic hydrogel due to no adhesion site for attaching.[39] However, bioinert is not suitable for cell encapsulation because of no adhesion site for target cells. Therefore, some DNA sequences are used to modify the backbone of synthetic polymer. Arginine-glycine-aspartate (RGD), which can be found in collagen, is the most common DNA sequence to improve the cell adhesion.[40-42] Moreover, PEG-peptide can also activate the inflammatory reaction so that anti-inflammatory DNA sequence is needed to introduce for modifying the backbone of PEG.[42] Another disadvantage of PEG is that the cross-linking of PEG is constructed by UV cross-linking. PEG precursor solution needs to mix with photoinitiator and then expose under UV light for cross-linking. Radical and chemical reagent would induce toxicity of cells, even kill cells during the cross-linking process. Table 1 shows the arrangement of advantage and disadvantage for natural and synthetic hydrogel.

Collagen is the most common materials for constructing extracellular matrix because it is abundant protein in human. Therefore, the biocapability and biocompatibility are the innate properties for collagen. Collagen fibers are constructed three polypeptide α-chains through entanglement of each polypeptide.[52] Figure 3 presents the schematic diagram for collagen fiber. Each polypeptide chain is composed by Gly-X-Y triplet repeatedly. Gly-X-Y triplet assists the interaction between three polypeptide through hydrogen bond. Collagen fiber can be classified as homotrimeric or heterotrimetic triple helices based on the composition of triplet. Homotrimeric collagen is constructed by repeated triplet, Gly-X-Y, to form fibrous structure, while, heterotrimeric collagen is composed by different triplets in fiber. Gauba and Hartgerink observed that the assemble heterotrimeric

collagen is combined by the mixture $(Pro\text{-}Lys\text{-}Gly)_{10}/(AspHypGly)_{10}/(ProHypGly)_{10}$ for 1:1:1 ratio.[53]

Table 1 Advantages and disadvantages of external cellular matrix using natural and synthetic hydrogel

<table>
<tr><th colspan="2">Hydrogel</th><th>Advantage for cell encapsulation</th><th>Disadvantage for cell encapsulation</th></tr>
<tr><td rowspan="3">Natural</td><td>Alginate</td><td rowspan="3">1. Abundance
2. Excellent biocompability
3. Biodegradable
4. Low immunogenicity</td><td>1. Inflammatory response[43,44]
2. Abnormal cell growth[45]</td></tr>
<tr><td>Chitosan</td><td>Weak mechanical property, Need to blend with other polymer to improve, like collagen[46,47]</td></tr>
<tr><td>Agarose</td><td>Temperature for solidification is high so that it’s difficult to operate for encapsulating cells.[48]</td></tr>
<tr><td colspan="2">Synthetic- PEGDA</td><td>1. Good mechanical properties
2. Suitable for micro fabrication
3. Bioinert (lower protein absorption)
4. Well-tuned structure function relations</td><td>1. No Adhesion site, Need to functionalize PEGDA with DNA sequence[49,50]
2. Inflammatory reaction, Need to functionalized anti-flammatory DNA sequence[50]
3. Radical and heavy metal polymerization will induce cytotoxicity[51]</td></tr>
</table>

Collagen fiber in human is cross-linking *via* hydroxylation at posttranslational modifications.[54] Numerous enzymes, like hydroxylases, collagen glycosyltransferases, peptidyl cis-trans isomerase and protein disulphide isomerase, assist the cross-linking, modification, folding in human in order to present biological function.[55] According to different modifications and functions of collagen, collagen can be categorized as 28

different collagens at least. The distribution of each type of collagen is shown in Table 2. Among these collagens, collagen type I is extremely applied in fabricating 3D microenvironment without imperfection and dominant in tissue. Other collagens would interrupt the triple helix structure as a result in blocking cell adhesion and signal transduction.[56]

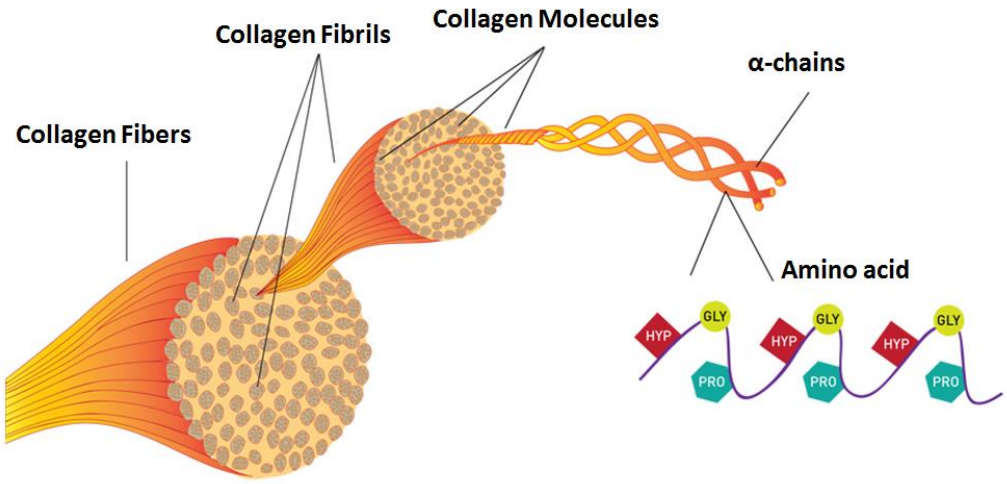

Figure 3 Collagen fiber structure. Collagen fiber is formed by triple helix collagen fiber in which the backbone of each collagen molecules is composed by Gly-X-Y. X and Y are any amino-acid, while Proline (Pro), Lysine (Lys), Asparitic acid (Asp), and Hydroporline (Hyp) are most common component for collagen molecules. (Reprinted from Ref. 53)

Collagen-based ECM is a good tool to mimic the progression for cancer study because large amounts of cancer properties are related to collagen fiber, such as migration and invasion.[57] Table 3 presents the researches using collagen-based ECM to realize the cancer properties. Therefore, owing to developing drug and treatment for patient, the interaction between cancer cell and matrix are important tools to recognize. Tumorigenesis is a multiple process characterized by (1) Limitless cellular proliferation

(2) cancer angiogenesis (3) invasion and metastasis. For example, cancer cell proliferation depends on the activation of the integrin β1, which can activate the FAK pathway. Brian et al. discovered that culturing MCF-7 in 3D collagen microenvironment can mimic and match *in vivo* model, especially for cell proliferation, cell viability, migration, and invasion. Moreover, they also used collagen-based 3D microenvironment to use as a validation platform for drug scanning.[58-59]

Angiogenesis is the formation of new capillary tube for obtaining oxygen and nutrient after metastasis. Kimlin et al.[60] discovered that co-culture of stromal cells and cancer cells in the same collagen-based 3D microenvironment can structure capillary-like microvasculature around cancer cells. This proves that the relationship between angiogenesis and interaction of cancer cells, collagen fiber and stromal cells. The mechanism of metastasis is hard to monitor because it occurred following circulation system. Therefore, collagen-based 3D microenvironment is used as tissue, and microfluidic system is designed as artificial blood stream. This integration under continuous flow enables to mimic the circulation system and realize EMT process during intravasation and metastasis.[61-63]

Table 2 The distribution of different collagen types presents in the human body. (Rewritten from Ref. 54)

Type	Class	Distribution
I	Fibril	Abundant and widespread in non-cartilaginous connective tissue: dermis, bone, tendon, ligament
II	Fibril	Cartilage, vitreous
III	Fibril	Co-distribution with collagen I: skin, blood, vessels, intestine
IV	Network	Basement Membrane (BM)
V	Fibril	Widespread and co-distribution with collagen I: bone, dermis, cornea, placenta
VI	Network	Widespread: muscle, bone, cartilage, cornea, vitreous
VII	FACIT	Dermis, bladder
VIII	Network	Widespread: dermis, brain, heart, kidney
IX	FACIT	Co-distribution with collagen II: cartilage, cornea, vitreous
X	Network	Hypertrophic cartilage
XI	Fibril	Co-distribution with collagen II: cartilage, intervertebral disc
XII	FACIT	Co-distribution with collagen I: dermis, tendon
XIII	MACIT	Endothelial cells, dermis, eye, heart
XIV	FACIT	Widespread and co-distribution with collagen I: bone, dermis, cartilage
XV	MULTIPLEXIN	Located between collagen fibrils that are close to BM, capillaries, testis, kidney, heart.
XVI	FACIT	Integrated into collagen fibrils and fibrillin-1 microfibrils, dermis, kidney
XVII	MACIT	Hemidesmosomes in epithelia
XVIII	MULTIPLEXIN	Associated with BM, liver
XIX	FACIT	Rate, localized to BM
XX	FACIT	Widespread: cornea (chick)
XXI	FACIT	Widespread: stomach, kidney
XXII	FACIT	Tissue Junctions
XXIII	MACIT	Limited distribution: heart, retina
XXIV	Fibril	Shares sequence homology with the fibril-forming collagens: bone, cornea
XXV	MACIT	Brain, heart and testis

Table 3 Collagen-based ECM used in cancer research

Crosslinking method	Cell source	Engineered 3D tissue models	Application	Reference
Thermogelation	NHEKs, NHDFS, SCC-12B and SCC13	Skin tissues	carcinoma progression	62
Thermogelation	ADSCs	Skin tissues	Evalulating vasculatizerd skin	63
Thermogelation	MCF-7, MYO 1089, HB4a, and HMFU19	Breast Cancer	Breast cancer progression	59
Thermogelation	MCF-10A	Breast Cancer	Breast cancer proliferation	65
3D collagen lattice	MDA-MB-231	Breast Cancer	ECM degradation for Cancer	66
Thermogelation	MDA-MB-231	Breast Cancer	Blood Circulation	61
Thermogelation	HMVEC	Vascular	human angiogenesis	60

1.4 Methodology for generating 3D microenvironment

Figure 4 shows the listed methodology for generating 3D microenvironment. 3D microenvironment can be created by hanging-drop,[68-71] bio-printing,[72] microfluidic device,[73] continuous flow lithography[74] and magnetic assembly levitation[75]. Hanging-drop is a good tool to make 3D microenvironment, especially for cell spheroid. Hanging-drop use surface tension around tiny holes to form droplet. Then, the suspended cells in droplet would force to aggregate and to form cell spheroid naturally.[68] Another method is for using pipetting to generate droplet manually.[69-70] However, hanging-drop approach is time consuming and labor-intensive process so that the production efficiency is relative low. Furthermore, the size distribution of cell spheroid is wide and the cell densities are not uniform.[71] Therefore, Hanging-drop system is not for wide-spreading. Bio-printing is a method to generate controllable process to eliminate the board variety of size uniformity. It integrated a simple, robust, and reproducible valve-based generator to print droplet out through adjusting voltage[76] or light.[77-79] Bio-printing is automatic and high-throuput system to generate 160 droplets per second. Compare to hanging-drop approach, the duration of preparation can be reduced as 600-fold.[72] However, cells cannot tolerate high temperature and stress during producing droplet via voltage or light so that the cell viability would be inhibited. Hung et al. designed microfluidic device to generate uniform 3D microspheroid for high throughput production.[73] Microfluidic device is design as flow focused microchannel. They use inertial force to make droplet in oil-to-water system. The size of microparticles are around 200 to 300μm. Microfluidic device can provide high-throughput of producing microparticles within uniform particle

size, however, oil phase around surface of microparticles would interrupt the function of encapsulated cells. On the other hand, oil phase would inhibit the cell function during the production of microspheres. Normally, 3D microenvironment has an issue for Insufficient diffusion of oxygen and nutrient would lead cells located at center part perform hypoxia and necrosis because of no vascular system. To overcome this problem, we can change the morphology of microparticles to improve the surface area to volume ratio. Higher surface area to volume ratio would enhance the diffusion rate of nutrient. The surface area to volume ratio for sphere is lower than the cube one. However, hanging-drop, bio-printing, and microfluidic device have limitation for producing non-spherical microparticles. Magnetic assembly levitation was also designed to produce non-spherical microenvironment.[75,80] Magnetic nanoparticles are encapsulated in polymer based microenvironment. Then, the formation of microparticles can be assembled into any shape of micro-cluster through controlling magnetic field and direction. However, the possible interaction between nanoparticles and cells would interfere the cell viability and its biological function. If the alternately current is applied, the local magnetic hyperthermia could also affect the cellular function and leads to destroy the structure of microenvironment.[81] Dendukuri et al. developed continuous flow lithography to make non-spherical micro-hydrogel.[74] They integrated the concept of microfluidic device and photolithography to make non-spherical microparticles. The polymer precursor, PEG solution, mixed with photoinitiator and then introduced into microfluidic device. Photomask within particles' pattern was placed underneath of microfluidic channel. Once the polymer precursor mixture passed through the exposing

area, solidification of PEG would occur at open area via photo-crosslinking. These PEG particles can be removed by flow after removing UV light. This system can be also used for mass production of non-spherical microparticles but the limitation is for material. Continuous flow lithography is integrated microfluidic device and photolithography. Therefore, continuous flow lithography is not allowed to synthesize non-photoinduced cross-linked polymer, like collagen.

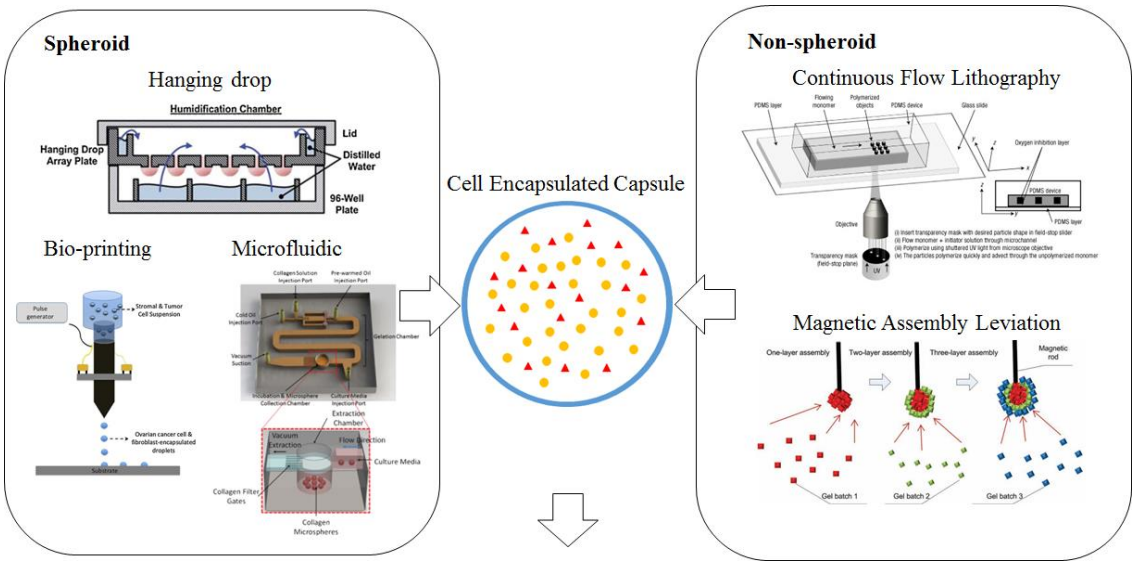

Figure 4 Methodology for making cell encapsulated capsule. Left side presents the method, hanging drop, bio-printing, and microfluidic system to generate spheroid capsule and right side shows the method, continuous flow lithography and magnetic assembly levitation to generate non-spheroid capsule

1.5 Morphology of Microenvironment

Based on the proliferation in 3D microenvironment, we can also distinguish as three zones, proliferating zone, quiescent viable cell zone, and necrotic zone, from outer layer to center of microenvironment.[83] Figure 5 presents the schematic diagram of typical zone

of cell proliferation in 3D microenvironment. These three zones are determined by the diffusion range of oxygen and nutrient. The diffusion limitation of about 150-200μm to many molecules, particularly for oxygen. Insufficient mass transportation leads to the accumulation of metabolic waste in the core so that a 3D microenvironment within 500μm size would display a layer-by-layer structure, which is called necrosis core, quiescent viable are and proliferation zone.[84] The morphology can be used to improve the diffusion efficiency through changing the morphology of microenvironment. The diffusion rate is proportional to the surface area. On the other hands, higher surface area can trigger faster diffusion rate.

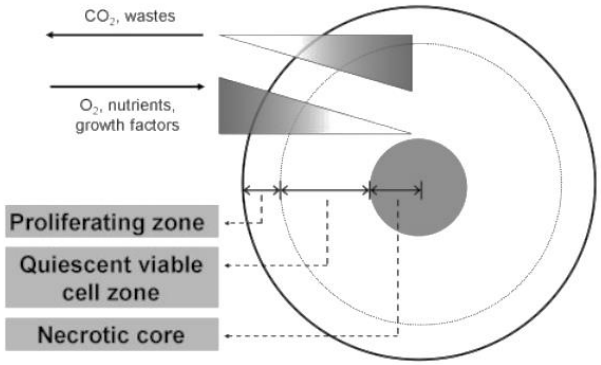

Figure 5 Schematic diagram 3D environment. 3D environment composed proliferating, quiescent and necrotic zone based on the mass diffusion of molecules. Proliferation zone is the region to perform low resistance of diffusion, while the necrotic core stands for the region presents high resistance of diffusion. (Reprinted from Ref. 84)

Table 4 is the comparison between different morphologies of particles. We collect sphere, triangle prism, and cubic particles for comparing their S/V ratio. The S/V ratio of spherical particles performs the lowest S/V ratio, which has 4.836, while the S/V ratio of

cubic particles presents 6. Except triangle prism and cubic particles, there is comparison between different morphologies shown in Figure 6 and they also mentioned the spherical particles have the lowest S/V ratio when the volume of each particles maintains constant. This result indicates that the diffusion rate can be improved through designing and creating different morphologies of particles. On the other hand, the necrotic core can be minimized and even eliminated by changing the particles' morphology. In this dissertation, we developed a device, called pneumatic actuated soft micromold (PASMO) device, which integrated pneumatic actuator and particles' template to create 3D cellular microenvironment. PASMO provides a controllable and gentle process to generate and extract cellular microenvironment within different shapes and sizes.

Table 4 Surface-to-volume ratios of sphere, triangle prism, and cube

Shape	Surface Area	Volume	Surface-to-volume ratio for unit volume
	$4\pi a^2$	$\frac{4}{3}\pi a^3$	4.836
	$(\frac{\sqrt{3}}{2}+3)a^2$	$\frac{\sqrt{3}}{4}a^3$	5.11
	$6a^2$	a^3	6

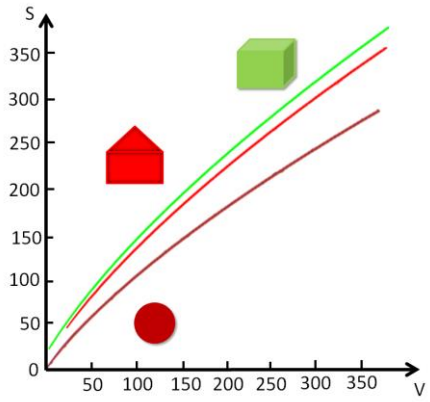

Figure 6 Surface area-to-volume ratio for different particles' shape. The spherical shape is more stable but it performed the lowest surface area-to volume ratio. This result interfere the diffusion of nutrients

2. DESIGN PNEUMATIC ACTUATED SOFT MICROMOLD*

2.1 Design of pneumatic actuated soft micromold (PASMO)

In this dissertation, we develop a system, pneumatic actuator soft micromold (PASMO) to produce non-spherical collagen microparticles for 3D environment. This system integrated soft microwell and pneumatic actuator. Pneumatic actuated soft micromold is inspired from Whiteside's group.[85] pneumatic actuator is composed two layers: top layer contained channel is for softer material and bottom layer is for stiffer material. In the beginning, the actuator does not deform due to the pressure difference between inside and outside is equal. Once the air is injected into air channel, the inside pressure is larger than atmosphere and then top layer would deform. However, the deformation of bottom layer is less than top layer because the mechanical properties are higher than top layer. Therefore, the obvious deformation is presented on top layer. Based on this result, we design three layers structure as a platform for extracting microparticles. The structure of pneumatic actuator soft micromold is constructed as three layers. Top layer is for soft microwells in order to making microparitcles and the middle layer is the air channel for actuation. The bottom layer is the stiffer material, which is used as resistance against the deformation from middle layer.

Figure 7 shows the strategy for actuation through pneumatic force and Figure 8 summarizes the process of extracting collagen microparticles from pneumatic actuated soft micro-molds. 3D collagen microparticles extraction process consists of five steps.

* Reprinted with permission from SOFT ROBOTICS, Year 2017, published by Mary Ann Liebert, Inc., New Rochelle, NY

Step 1: Preparation of collagen solution and dispensing collagen solution into molds. Collagen for creating 3D microenvironment is collagen type I, which is extracted from rat tail. Collagen dissolves in 1% acetic acid and the concentration is 3.5 mg/mL. Neutralized collagen can be filled in each particles' wells.

Step 2: Cross-linking of collagen particles. The whole device is placed in incubation at 37^{o}C for 5 to 10 minutes for curing collagen.

Step 3: Rinsing process. The whole device is merged into 1x PBS or culture media after curing.

Step 4: **Air injection and expansion of particles' wells**. Air is pumped into pneumatic soft micromold device for expanding particles' wells. As pressure is increasing, micro-patterns enlarge and PBS or culture media would diffuse into small gaps between collagen microstructures and molds.

Step 5: Floating and pushing of collagen particles. Collagen particles start floating because large amount PBS or culture media is diffused into individual molds. In addition, the bottom of PASMO is simultaneously extruded to push collagen particles and they are released into PBS or culture media.

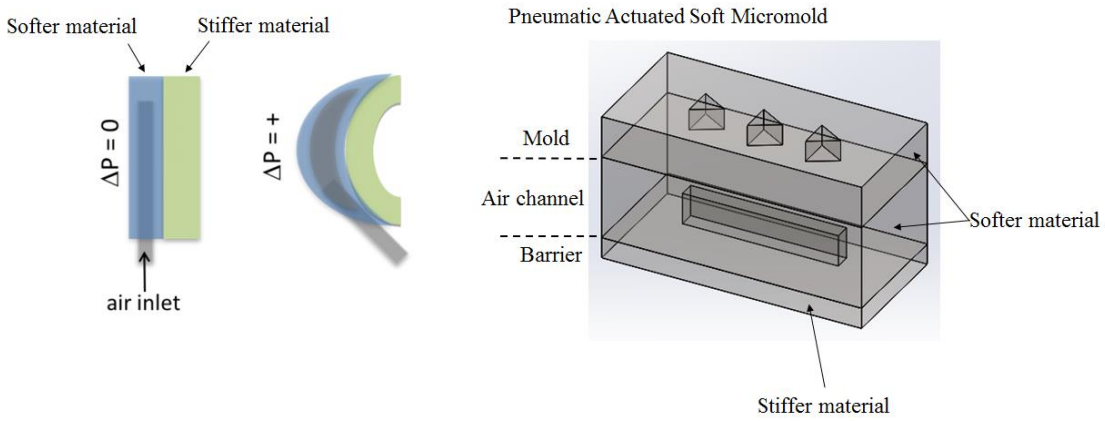

Figure 7 Mechanism of pneumatic actuated soft micromold and its structure. Right side presents the working strategy for pneumatic actuator, which composes soft material on top and stiff material at bottom. Top layer would perform obvious deformation. Left side is the schematic diagram for pneumatic actuated soft micromold (PASMO) and its structure, particles' template, air channel and resistance

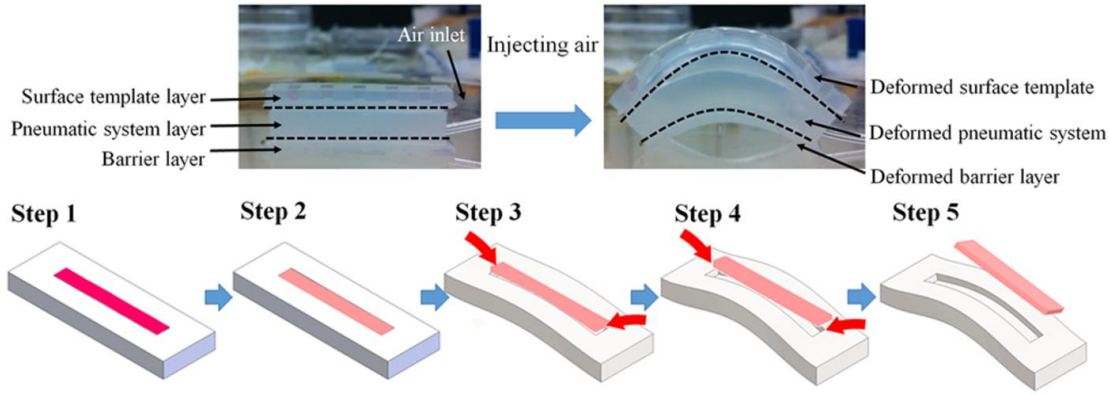

Figure 8 Schematic diagram of collagen microstructure production process *via* PASMO device. There are five steps for this extraction process 1: Dispensing collagen solution into molds; Step 2: Cross-linking of collagen microparticles; Step 3: Rinsing process; Step4: Air injection and expansion of micro-mold; Step 5: Floating and pushing of collagen microparticles

2.2 Fabrication process of pneumatic soft micromold device (PASMO)

The fabrication process of PASMO device is shown in Figure 9(a-d). The master-mold for the surface template layer is made via the standard photolithographic process with SU8 photoresist as described previously.[86-87] A PDMS solution is spin-coated on the master-mold and cured at 65 °C for 2 hours, then, peeled from the master-mold (Figure 9a). The master molds for the pneumatic system and barrier layers are made by Envision tech 3D printer. Un-cured Ecoflex-30® is poured over a pneumatic system mold and cured for 4 hours at room temperature, and peeled from the mold (Figure 9b). The width and depth of channel inside the pneumatic system layer are 1.5 mm and 3.0 mm, respectively. A cleaning cloth with high tensile stress is placed inside the barrier layer mold and encapsulated in this layer; then, uncured Ecoflex-30® is dispensed over the cloth in the mold. Ecoflex-30® is cured at room temperature for four hours and peeled from the mold (Figure 9c). Surface template, pneumatic system and barrier layers are subsequently bonded at 65^{o}C for two hours with uncured Ecoflex-30® used as glue between layers (Figure 9d). The image of PASMO device with a tube attached for applying pneumatic pressure is shown in Figure 9e.

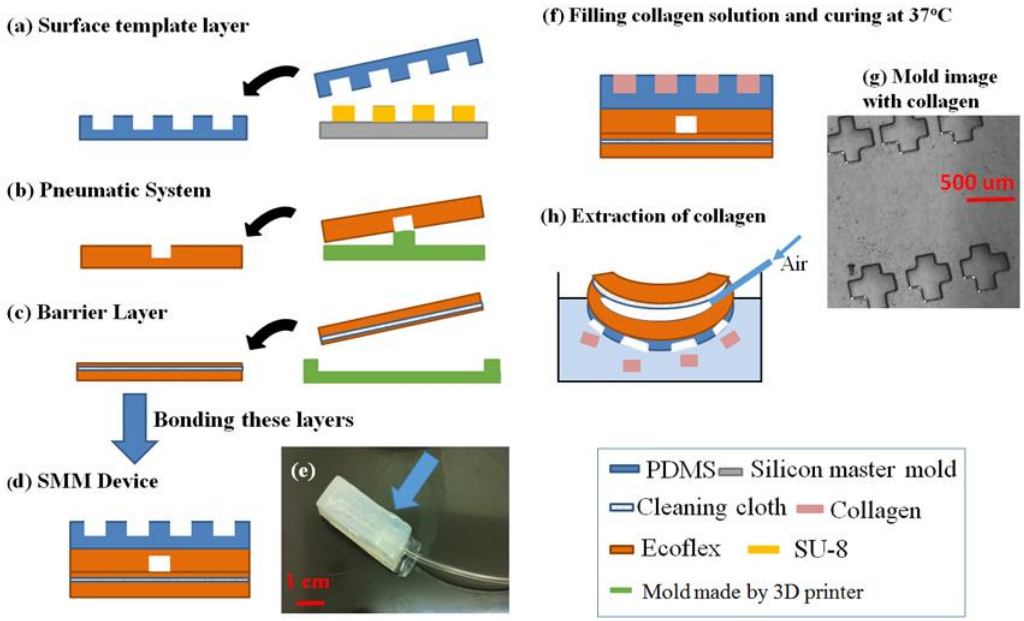

Figure 9 Schematic diagram of fabrication process for Soft micro mold device. Molding process of (a) surface template layer (b) pneumatic system layer (c) barrier layer. (d) The bonding process of these three layers. (e) Photographic image of PASMO device with tygon tubing. (f) Collagen microstructure fabrication process. Filling collagen solution into surface templates and curing at 37°C. (g) Microscopic image of micro scale surface templates of cross prism shape. (h) Collagen microstructure extraction process with pneumatic actuation. This is side view as shown the arrow in Figure 9e

3. CHARACTERIZATION OF PASMO*

3.1 Photographic image and operation for soft micromold device

Figure 10 shows the photographic image of entire pneumatic soft micro mold (PASMO) device, which consists syringe pump and PASMO device that are connected by tygon tubing. Pneumatic pressure is applied to PASMO device by compressing syringe, as a result, the micro-mold is extended and deformed as convex shape. The pressure to optimize the deformation of PASMO device and extraction of collagen microstructures is set as 1.1, 1.2, 1.7, 2.0 and 2.5 atm.

Figure 10 Photographic image of pneumatic actuated soft micromold device. Pneumatic actuated soft micromold (PASMO) device is consisted with syringe, micromold and connecting Tygon tube

3.2 Characterization for deformation of patterns on PASMO device

The deformations of PASMO devices are the key to clean extraction of collagen micro-structures; therefore, it is important to characterize the deformations of individual micro-patterns by pneumatic actuation. Figure 11 shows the microscopic images of

* Reprinted with permission from SOFT ROBOTICS, Year 2017, published by Mary Ann Liebert, Inc., New Rochelle, NY

cross-shaped micro-patterns on PASMO devices with the pressure application from 1atm (no pressure) to 2.5atm, while Figure 11a-f consists of the schematic diagram of 3D deformation of micro-pattern. The scaled expansion rate defined as $(W_0-W_1)/W_0$, (W_0: the initial width of pattern, W_1: the pattern width after injecting air) for the cross shape micro patterns in X width at the position 1 to position 5 in Figure 11B are 10%, 35%, 108%, 78%, and 81%, respectively with 2.5 atm pressure application. The graph of the expansion rate of cross-shaped micro-pattern in X width as function of applied pressure is shown in Figure 11-a. The highest expansion rate of micro-mold is observed at the position 3 at Figure11-f. The Y width is also expanded 16%, 18%, 60%, 31 % and 47% at the position 1 to position 5 in Figure 1B, respectively with 2.5 atm pressure application. The averaged expansion rate from positions 1-5 in X width is 62.4% that is higher than one in Y width (60%) shown in Figure 11B-b. The expansion rate in X and Y width is determined by the design of channel network and it can be easily improved by the channel network design. In addition to X, Y width, the depth of micro-pattern is reduced linearly from 100 μm to 56 μm with pressure increased as shown in Figure 11D. This Z directional extrusion from the bottom of micro-pattern increases the successful rate of microstructure extraction process. The expansion rate of micro-pattern on the surface template layer is linearly proportional to the pressure application. In addition, expansion of micro-pattern and extrusion of bottom of micro-pattern improves the extraction of collagen microstructures from micro-patterns.

3.3 Preparation of collagen microparticles through PASMO device

The concentration of the rat-tail collagen type I solution is set to 3.5 mg/mL for the entire set of experiments. This collagen solution is dispensed into the surface templates and gelled under the neutral condition (pH =7.4) at 37^{o}C for one hour (Figure 9f). The microscopic image of the surface layer with the collagen solution is shown in Figure 9g. Pneumatic pressure is applied to the pneumatic channel from a syringe pump, which leads to the deformation of PASMO devices and the subsequent release and harvest of collagen microstructures in PBS, as shown in Figure 9h. Due to the high tensile stress of the cleaning cloth inside the bottom layer, the PASMO device deforms asymmetrically with the surface layer expanding the most while the bottom remains intact, which promotes the extraction of collagen microstructures from the surface template layer.

Figure 12 presents the microscopic images of collagen microstructures of cross column (Figure 12a), pentagonal prism (Figure 12c), hollow cylinder (Figure 12e), triangular prism (Figure 12g), and square pad (Figure 12i) produced via PASMO devices. Then, in order to characterize the size reproducibility, the dimensions of the structures are compared to those of mold patterns (Figure 12b, d, f, h and j). The results show an approximately 96% accuracy for each microstructures ranging from 100 to 1000 μm, as shown in Figure 12k. On the other hand, the reproducibility of collagen microstructures smaller than 100 μm is limited, as the collagen solution is not completely dispensed into micro patterns. The thickness of microstructures is set to 100 μm for all structures and is duplicated with more than 92% accuracy as shown in Figure 13. Compared to manually pushing gelled collagen particles from the micro-patterns by

hand, the extraction forces in PASMO devices are easily controlled and can extract fragile collagen structures from molds by applying an incrementally bigger volume of air into the pneumatic channel. The successful extraction rates of micro cross-collagen by the PASMO device and manual pushing approach are 95% and 15%, respectively, as shown in Figure 14. Figure 14 further demonstrates the structural damages observed among those collagen microparticles extracted manually by hand. It shows microscopic images of collagen micro-cross-columns extracted by soft micro-mold (PASMO, Figure 14A) device and traditional manual pushing (Figure 14B), respectively. Collagen micro-cross-column extracted by PASMO device maintains dimensions and shapes. Micro cross columns extracted by manual pushing is normally damaged as shown in Figure 14B. The successful extraction rate for both approaches are shown in Figure 14C. It is obvious that PASMO device demonstrate significantly better extraction success data that improves reproducibility of collagen microstructure production.

Figure 12l shows the result of second harmonic generation (SHG) microscopic images of collagen micro-cross column to characterize their collagen fiber structures. The density of collagen fiber distribution is determined using Image J to be 86.57%, which is higher than that of collagen microspheres produced in microfluidic devices (62.45%)[88-94]. This matches the density range of collagen fiber in dermis, bone, tendon and ligament (72-94%).[95] In addition, the relatively dense collagen microstructures can remain intact when they are injected into an agarose gel without being damaged, unlike their less dense collagen microsphere counterparts, as shown in Figure 15.

It shows the comparison collagen microstructures made by PASMO device and microfluidic emulsion process before and after injection through 19 gauge syringe needle. Microscopic images of collagen microparticles made by microfluidic device and micro cross-prism made by PASMO devices are shown in Figure 15A and C before the injection to agarose gel. Microscopic images of these microstructures after injections are shown in Figure 15B and D after injection process through 19 gauge syringe into agarose gel. Collagen microspheres are fragmented and merged other after injection process even with surfactant during this injection process. (Figure 15B, D) While collagen micro-cross column made by PASMO device overcome the pressure drop during injection process to agarose gel, the shape and the size of collagen micro-cross-column are maintained same as the original ones. (Figure 15C, D). Second harmonic generation (SHG) microscopic images of microstructures made by these two approaches are shown in Figure 15E and F The collagen fiber density of these two microstructures are calculated by Image J and shown in Figure 15G. This demonstrates that collagen microstructures made by PASMO devices are suitable for implantable 3D tissue engineering applications.

In addition, collagen microstructures produced by PASMO devices maintain their dimensions and shapes, with no observable shrinkage or expansion in size over 50 hours (Figure 12m). Thus, PASMO devices are able to precisely control the dimensions and shapes of collagen microstructures. These collagen microstructures are stored in the 4 °C refrigerator for up to 60 days without any shape changes.

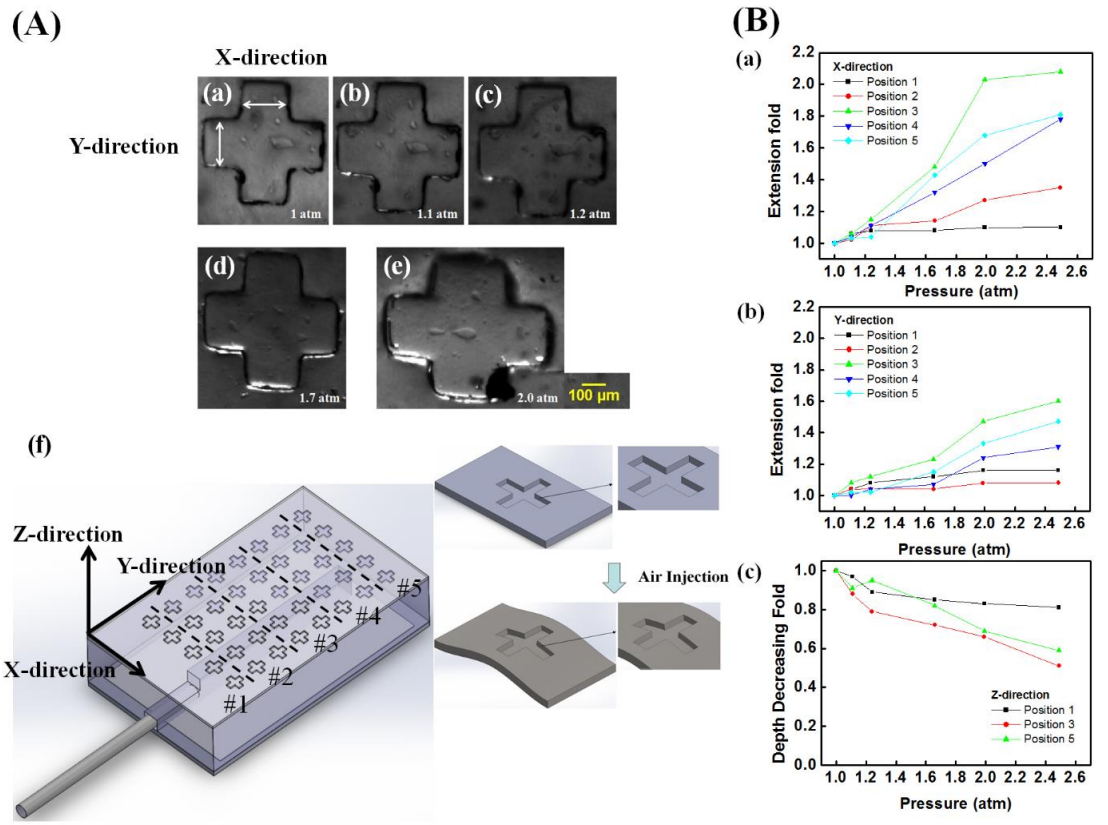

Figure 11 Deformation of micro-pattern on PASMO device with pneumatic actuation. (A). Microscopic images of micro-patterns with pressure application. (a) 1 atm (no injection of air) (b) 1.1 atm (0.2 mL injection) (c) 1.2 atm (0.4 mL air injection) (d) 1.7 atm (0.8 mL air injection) (e) 2.0 atm (1 mL air injection) of pressure are applied. Scale bar is 100 μm for all images. (f) Schematic diagram of PASMO device (B). The deformation of soft micro-patterns at x, y-width and z-direction based on their location on PASMO devices shown in Figure 11f

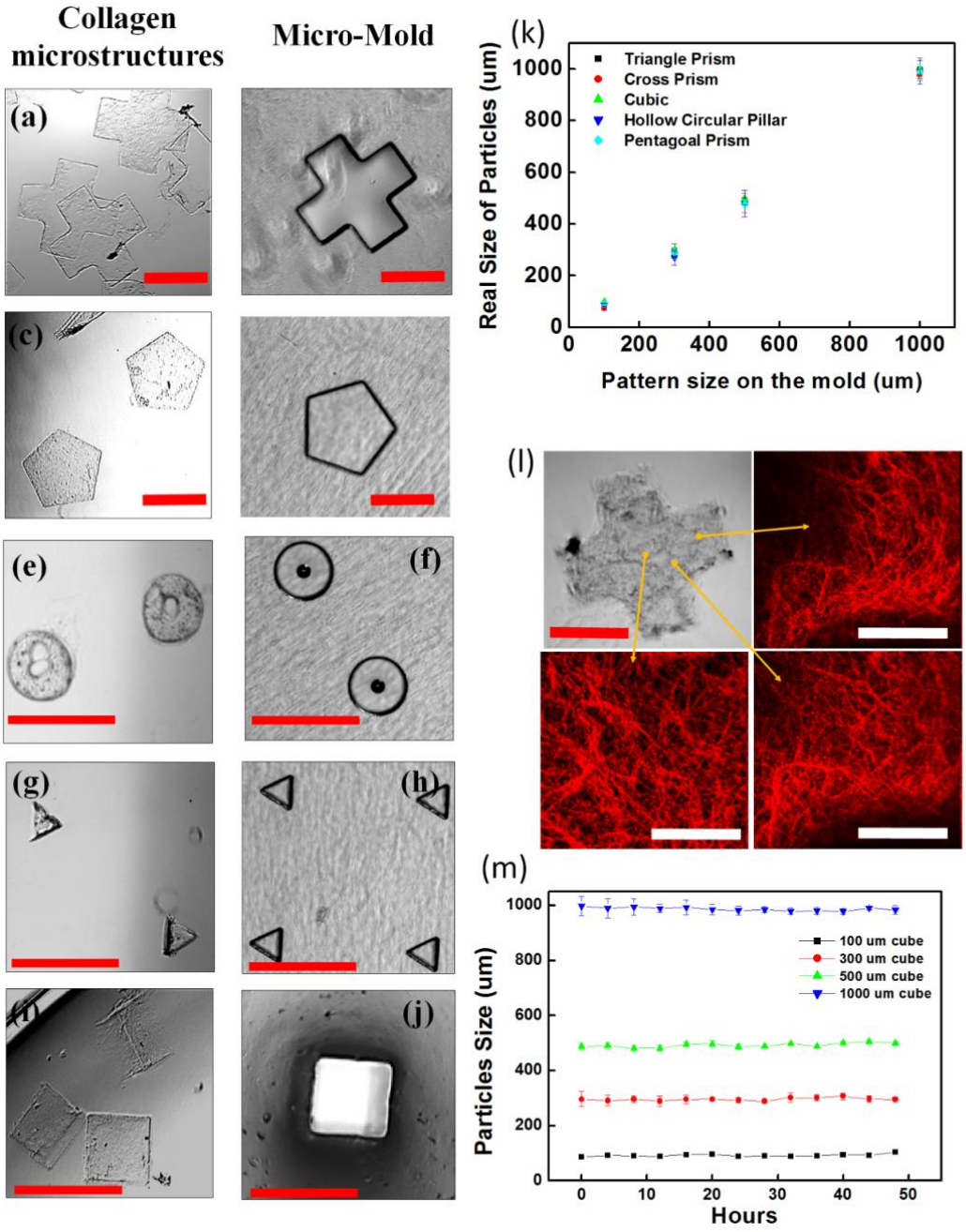

Figure 12 Characterization of collagen microstructures made by PASMO device. Microscopic images of microstructures and molds for (a-b) cross column, (c-d) pentagonal column, (e-f) hollow circular cylinder, (g-h) triangular column, (i-j), square pad, respectively. The thickness of these microstructures are set to 100 μm. (k) Duplication accuracy as function of dimensions of micro molds. (l) Second harmonic generation microscopic image of collagen fibers in micro cross column. (Red and white scale bar are 500, 100 μm, respectively.) (m) Dimensions of collagen micro-cubes as function of times after productions

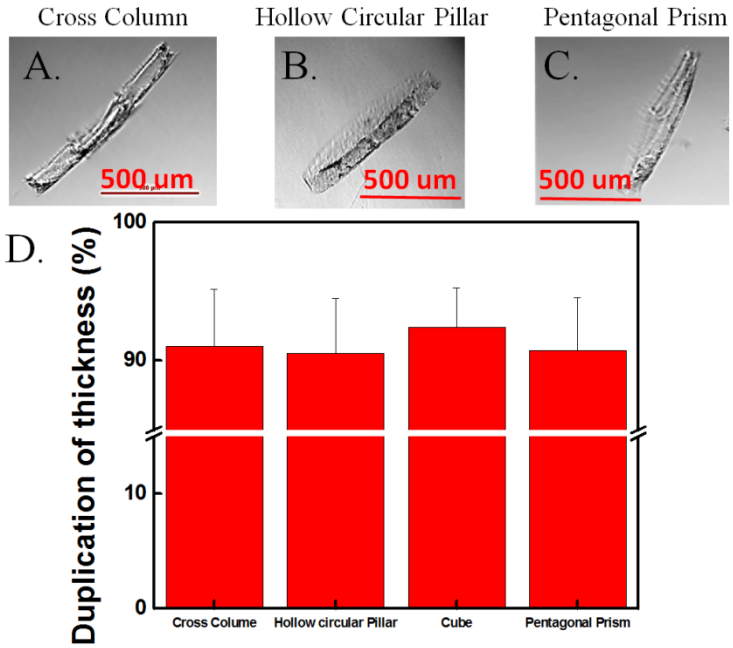

Figure 13 The thickness of collagen microstructure. Side view of (A) Cross Column (B) Hollo Circular Pillar (C) Pentagonal Prism (D) Duplication of thickness for collagen microparticles with cross column, hollow circular pillar, cube and pentagonal prism

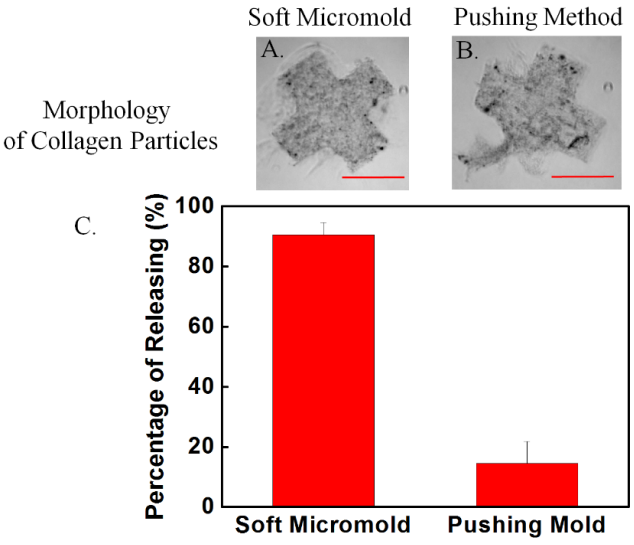

Figure 14 Collagen microstructures extracted from mold patterns by (A) PASMO device, (B) manual pushing. (C) The graph for microstructure extraction success rate between PASMO device and manual pushing approaches. The scale bar is 500 μm.

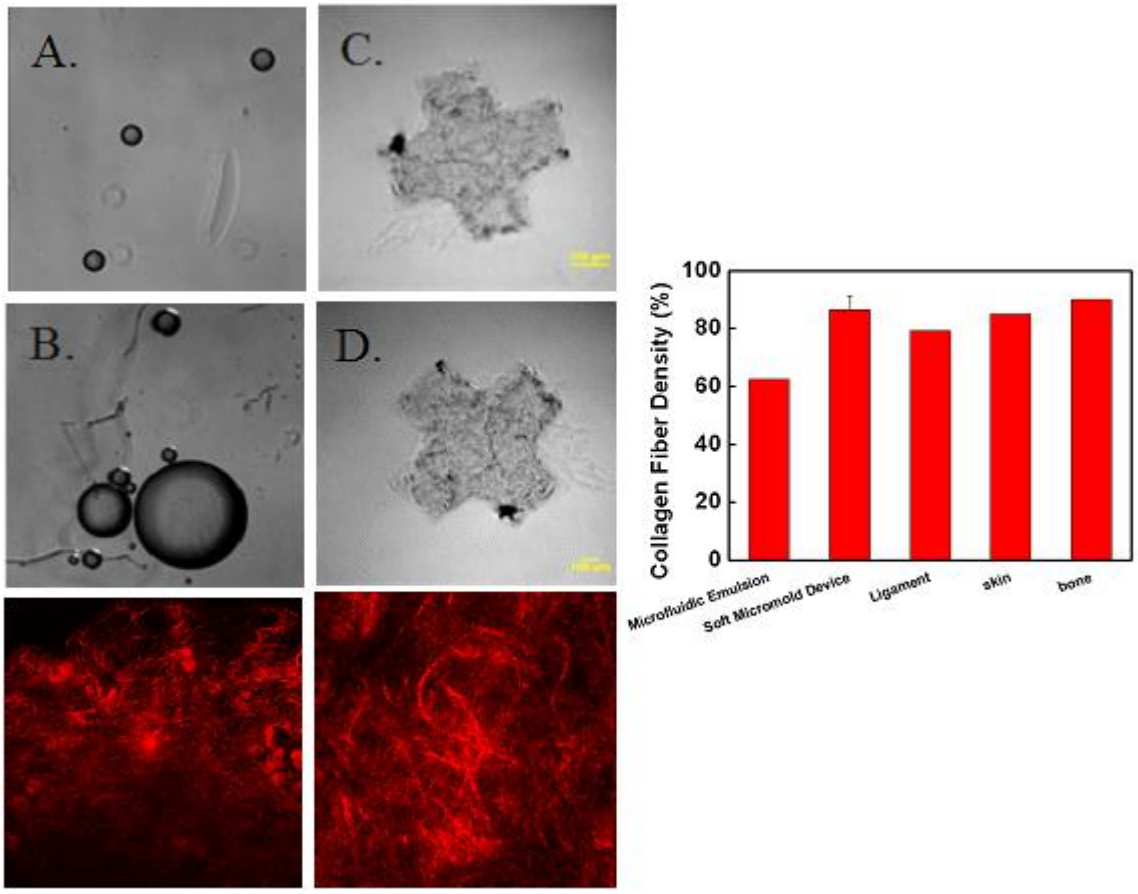

Figure 15 The effect of injection of collagen microstructures made by microfluidic emulsion and soft micro mold device. Collagen microspheres made by microfluidic device (A)before and (B) after injection. Collagen micro cross column made by soft micromold (PASMO) device (C). before and (D) after injection. (E)SHG microscope image of (F) collagen microparticles made by microfluidic and of (G) micro-cross column made by PASMO device

4. CANCER IN 3D MICROENVIRONMENT*

4.1 Preparation of collagen microparticle contained MDA-MB-231

The PASMO device also produces collagen microstructures encapsulating MDA-MB-231-GFP cells that overexpress Green Fluorescence Protein (GFP) as long as they are viable. The cellular concentration for all experiments is set to 10^6 cell/mL. The cellular proliferation and contraction of collagen microstructures are investigated as potential collagen modular microenvironment. For cell encapsulation inside collagen micro-structures, MDA-MB-231-GFP cells overexpressing Green Fluorescent Protein (GFP) are mixed with a 3.5 mg/mL collagen solution as previously described and dispensed into surface templates.[96-98] Collagen microstructures with embedded cells are released from the deformed surface template layers of PASMO devices into Dulbecco's Minimal Essential Medium (DMEM) with 10% fetal bovine serum (FBS). Cells inside collagen microstructures are cultured in a humidified incubator (5% CO_2 and 95% air condition) at 37^{o}C for more than 14 days.

Figure 16a shows fluorescent images of MDA-MB-231-GFP cells encapsulated in collagen micro-cubes for 0, 4, 8 and 12 days. The fluorescent intensities in the micro-cube and normalized micro-cube volume as a function of days are also plotted in Figure 16b. Bright spots on the surface or inside of the collagen structures correspond to MDA-MB-231-GFP cells. Over time, the fluorescent signal tends to increase in intensity, indicating the proliferation of MDA-MB-231-GFP cells in collagen micro-cubes and remains for more than 14 days. The volumetric shrinkage of collagen micro-cubes is also

* Reprinted with permission from SOFT ROBOTICS, Year 2017, published by Mary Ann Liebert, Inc., New Rochelle, NY

significant after the 4^{th} day due to the increase in the number of cells. Figure 16c presents the volumetric shrinkage of collagen micro-cubes. Cancer cells generate contractile force in order to rearrange the collagen orientation. We encapsulate MDA-MB-231-GFP cells in collagen micro-cubes with 300, 500, and 1000 um, respectively. And the concentration of cells is set to 10^6 cells/mL. After 7 days, the volume of micro-cubes would remain 40% of original size. There is no difference of contraction ratio among these three different sizes of micro cubes.

In addition, Figure 16a, c shows the volumetric shrinkage of collagen micro-cubes containing cancer cells as a function of days for three sizes of micro-cubes (1000 μm, 500 μm and 300 μm). There are no significant differences among them because the number of cells per unit volume is set to be constant. Figure 16c show fluorescent images of the micro-cross column encapsulating cells on day 0, 3 and 7. From Day 0 to Day 3, they are slightly contracted comparing to the originals; by Day 3, the volumetric shrinkage is around 22%. Between 3^{rd} to 7^{th} days, the structure shrinks significantly by 60%. The micro-cross column is deformed irregularly from the original one, unlike the shape-steady micro-cubes, which suggests an existence of an interesting shape-dependent shrinkage behavior. To extend the application of collagen-based 3D microenvironment to clinical test, high throughput is the key requirement. The 1^{st} generation of PASMO is constructed on the straight channel. However, the most deformed area occurred at the center part from the result from either experiment or simulation. While, there is less deformation around edge part. On the other hand, collagen particles locating at edge part are not easily extracted from microwells.

Therefore, we design 2nd generation of PASMO. Figure 17 present the design of 2nd generation of PASMO. The 2nd generation of PASMO is also composed by three layers, which are microparticles template, channel layer, and resistance layer, as top, middle, and bottom layer, respectively. The only different design is the shape of channel and the shape is designed as circular shape instead of straight channel. We use Ogden model to simulate the deformation of PASMO within straight and circular design.

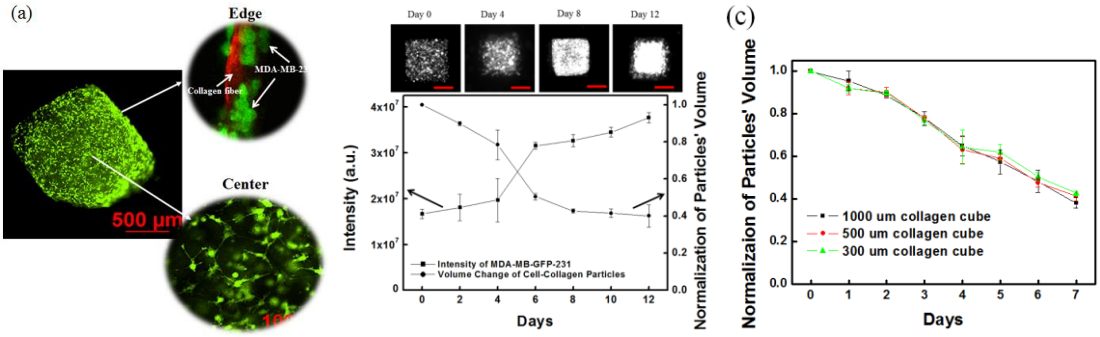

Figure 16 MDA-MB-231-GFP Cell-collagen microparticles. (a) Cell morphology in collagen microparticles (b) Fluorescent microscopic images of micro-cubes containing MDA-MB-231-GFP cells at day 0, 4, 8, 12. The graphs for fluorescent intensity and volumetric shrinkage of collagen micro cubes as a function of days. Scale bar is 500μm. (c) The volume shrinkage of collagen micro-cube with 300, 500, and 1000μm dimensions as function of days

4.2 Simulation of Pneumatic actuated soft micromold

The Ogden material model is a hyperelastic material model used to describe the non-linear stress-strain behavior of complex materials such as rubbers, polymers, and biological tissue. The model was developed by Ray W. Ogden in 1972.[99] The Ogden model, like other hyperelastic material models, assumes that the material behavior can

be described by means of a strain energy density function, from which the stress–strain relationships can be derived.

$$U = \sum_{i=1}^{N} \frac{2\mu_i}{\alpha_i^2}(\bar{\lambda}_1^{\alpha_i} + \bar{\lambda}_2^{\alpha_i} + \bar{\lambda}_3^{\alpha_i} - 3) + \sum_{i=1}^{N} \frac{1}{D_i}(J^{el} - 1)^{2i}$$

$$where \mu_i, \alpha_i, N, and\ D_i\ are\ material\ cofficient$$

$$\bar{\lambda_J} = J^{-1/3}\ for\ j = 1,2,3\ J\ is\ the\ volume\ ratio$$

Shear modulus (G) can be determined by

$$G = \sum_{i=1}^{N} \mu_i\ for\ silicone, N = 1$$

Poission Ratio can be calculated by D_i and G

$$D_1 = \frac{3}{G}\frac{(1-2v)}{(1+v)}$$

μ_1=0.011114056, μ_2=1.119657985E-005, μ_3=0.01144378401

α_1=2.39364222, α_2=8.1236594, α_3=-2.16818767

Figure 17b shows the simulation result, which indicate that all wells would deform after increasing inside pressure. Compare to the straight channel, circular design would effectively eliminate the edge effect of straight channel. Moreover, the deformed height and area is also improved in circular design, especially for expanded area. Figure 18 demonstrated that the expanded area is changed from 10 mm^2 to 27 mm^2 under the pressure at 0.04MPa. On the other hand, culture media or buffer solution can be easy to fill in expanded microwells in order to float microparticles out. 2nd generation PASMO is not only effectively eliminate the edge effect but also improve the production rate for making collagen-based 3D microenvironment.

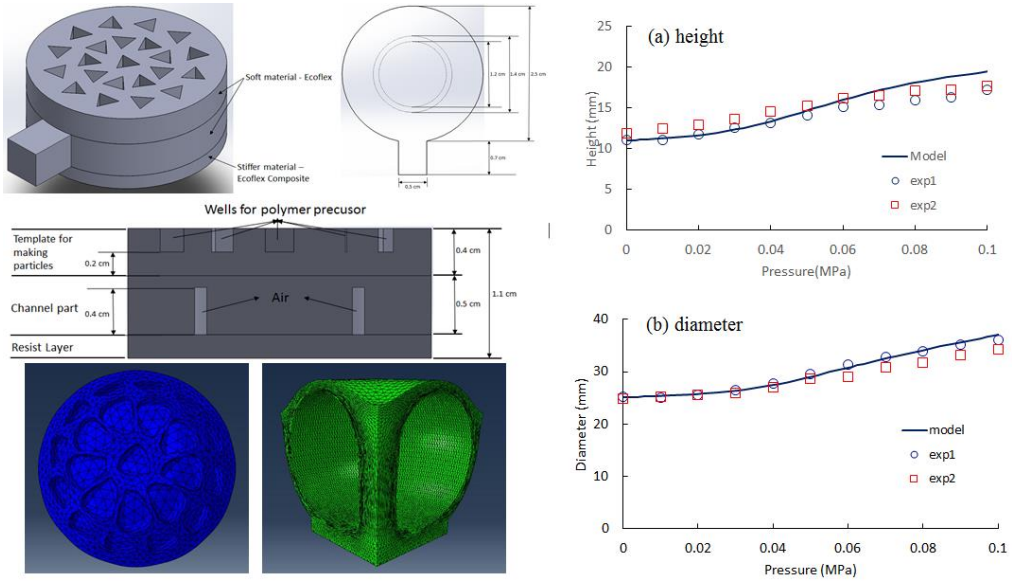

Figure 17 The schematic diagram for PASMO (a) Whole image of PASMO (b) PASMO is composed by three layers, template, channel, and resist layer (c) The working of PAMS before and after air injection

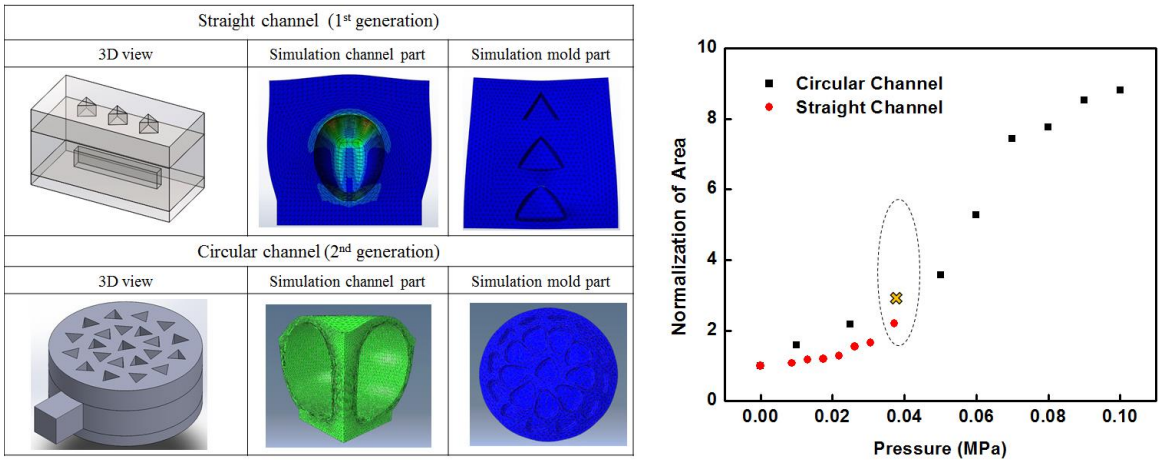

Figure 18 Comparison between straight channel design and circular channel design. The table arranges the straight channel and circular channel within 3D view, simulation of channel part and mold part, respectively. Compare to the expanded area, the circular design can perform higher expansion.

Collagen-based 3D microenvironment is more close to in vivo study because the scaffold based cultures has additional interaction between cells and matrix, which lose in cellular spheroids. Moreover, the cellular complexity in scaffold-based cultures is much higher than cellular spheroids. Many researches also mentioned drug candidates lose efficiency in a 3D microenvironment compare to 2D and cellular spheroids. (Figure 19)[100-102] Herein, we treated paclitaxel to MDA-MB-231-GFP in collagen-based 3D microenvironment and monitor the drug effect over 7 days.

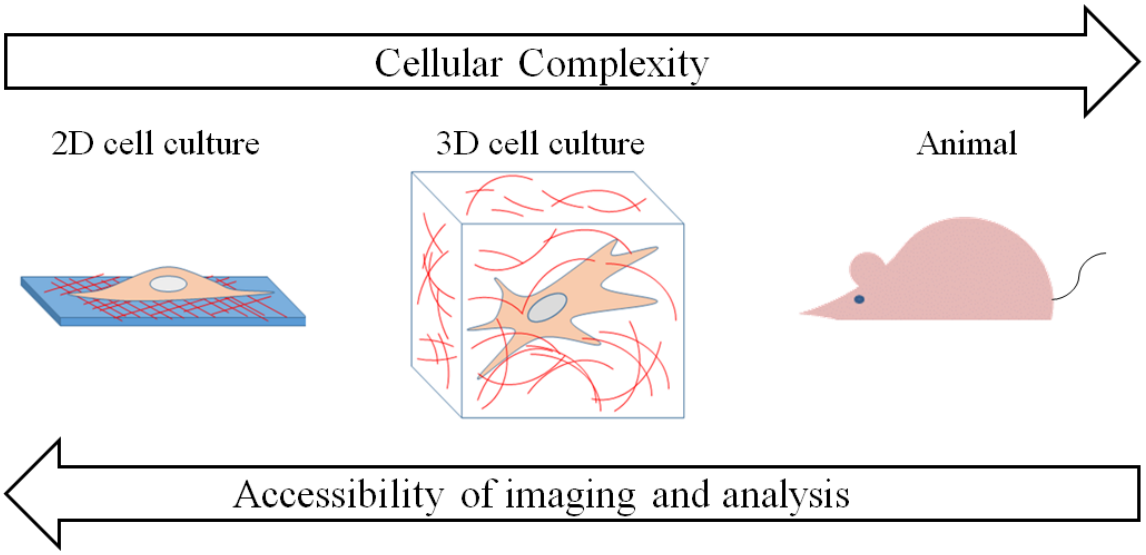

Figure 19 Rethinking drug screening processes. Tissue engineering provides 3D cultures that recreate the complex cellular microenvironment more precisely than traditional 2D cultures, due to the incorporation of multiple physical, mechanical and chemical cues that arise from ECM-cell and cell-cell interactions. At the opposite end of the experimental continuum, animals do not capture important facets of human behavior and they are not feasible for HTS applications. Therefore, 3D cultures can bridge the gap between 2D cultures and animal models. (Redrawn from Ref. 100)

4.3 Collagen-based 3D microenvironment for sensing of Paclitaxel

Figure 20 presents the mechanism of Paclitaxel for defeating cancer cells. Paclitaxel is a well-known anti-cancer drug and its mechanism is to block the chromosome segregation through damage the mitotic spindle. This inhibited function is general to contribute its suppression of DNA duplication so that the mitosis would be interrupted. As a result, cancer cells would trigger the apoptosis process and lose their biological function.[103-107] On the other hand, the contractile force of cancer cells would be eliminated after treating paclitaxel. Therefore, we can observe the shrinkage of collagen-based 3D microenvironment under different concentrations of Paclitaxel.

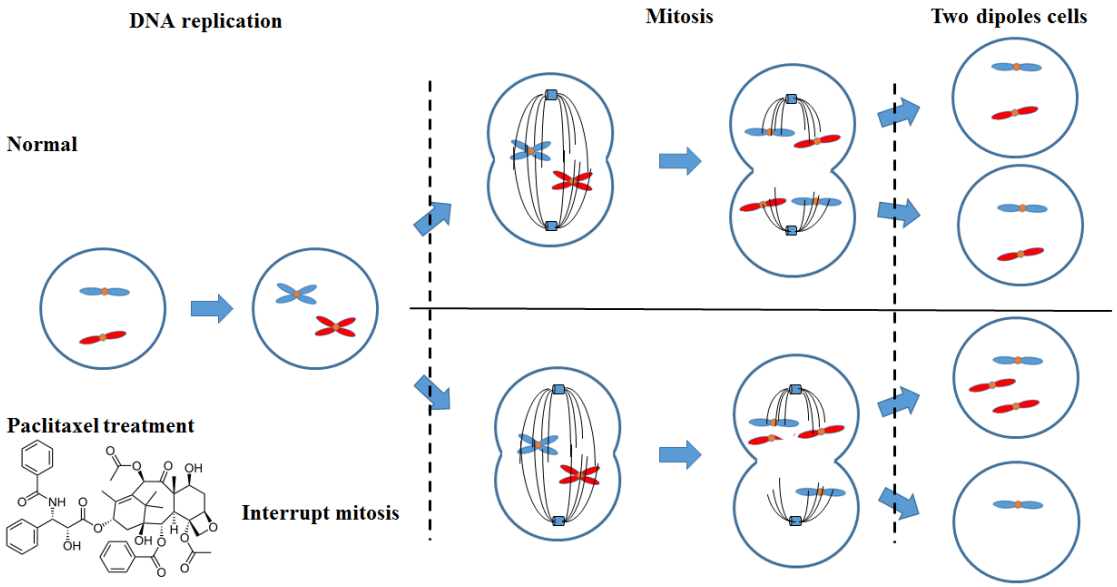

Figure 20 The mechanism of Paclitaxel for treating and inhibiting the survival of cancer cells. Paclitaxel inhibit the activity of mitotic spindle in order to destroy the mitosis. Abnormal dipoles cells would generate and trigger apoptosis process. (Redrawn from Ref. 103)

Collagen microparticles encapsulating cancer cells are exposed to 1, 0.1, and 0.01 μM concentrations of paclitaxel solutions. Cell proliferation and the size of collagen microstructures are investigated over 7 days. Figure 21d, e and f show fluorescence images of collagen micro-cubes exposed to paclitaxel with concentrations of 1, 0.1, and 0.01 μM on days 0, 3 and 7. Paclitaxel is a commonly used anti-cancer drug, and it stabilizes cellular microtubules that terminate the contraction of MDA-MB-231-GFP in collagen.[108] The volumes of collagen micro-cubes reduce to 40, 50, and 67% of original size with paclitaxel concentrations of 1, 0.1, and 0.01 μM, respectively, on the 7th day. Compared to micro-cubes without paclitaxel, micro-cubes exposed to 0.1 and 1 μM have far less overall volumetric shrinkage. On the other hand, micro-cubes with 0.01 μM paclitaxel have almost the same volumetric shrinkage rate as micro-cubes without paclitaxel due to less stabilization of microtubules among cancer cell. The volumetric shrinkage ratio for collagen micro-cubes without cells, collagen micro-cubes and cross-columns with cells, micro-cubes with cells exposed to paclitaxel as a function of days are all plotted in Figure 21g. Colby et al. also observe that paclitaxel can inhibit the cancer growth in 3D microenvironment.[109] Compared to control (without treating paclitaxel), the size of microenvironment is larger than control group. It indicates that biological function can observe the inhibition of cancer cell growth and can monitor the surrounding stimuli in 3D microenvironment.

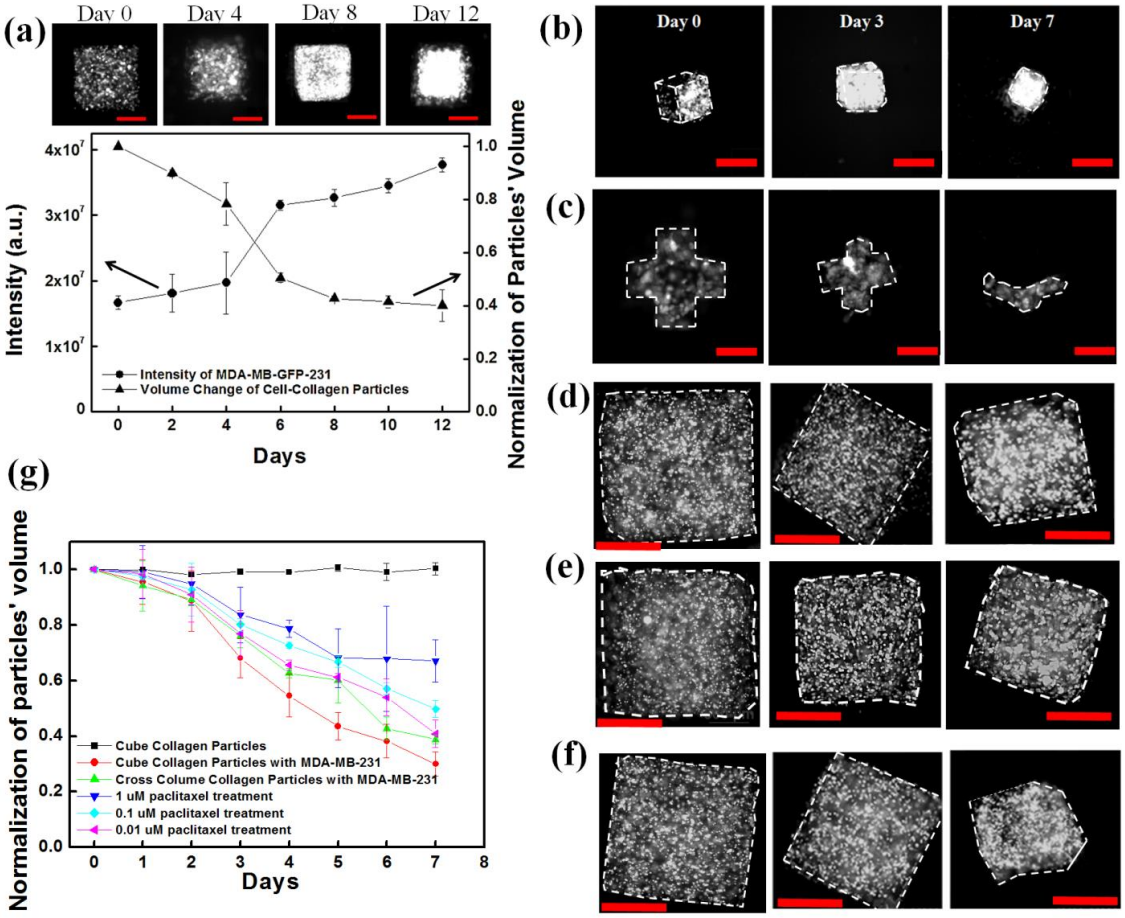

Figure 21 MDA-MB-231-GFP Cell-collagen microparticles (a) Fluorescent microscopic images of micro-cubes containing MDA-MB-231-GFP cells at day 0, 4, 8, 12. The graphs for fluorescent intensity and volumetric shrinkage of collagen micro cubes as a function of days. Scale bar is 500μm. Fluorescence microscopic images of (b) micro-cubes, (c)micro-cross column, micro cubes containing MDA-MB-231-GFP cells exposed to (d) 0.01, (e) 0.1, and (f) 1 μM paclitaxel at day 0, 3 and 7. Scale bar is 500 μm.

Moreover, collagen-based 3D micropartilces creating from PASMO can be applied in cancer xenograft. Cancer xenograft plays a crucial role for cancer treatment because of discovering drugs and finding suitable treatment for patients.[110] The widely method for setting cancer model is to mix scaffold with cancer cell line and then inject into nude mice in vein. The disadvantage of injection of vein is that cancer cells cannot be housed at specific location. If the number of cells at specific location is not high enough, the

tumor cannot be formed easily. PASMO overcomes this problem because it can generate microenvironment for cancer cells, especially extremely soft material, like collagen or Matrigel™.

Figure 22 present the procedure for cancer xenograft and Matrigel™ is the target material for cancer xenograft. Matrigel™ is derived from reconstituted basement membrane form the Engelbret-Holm-Swarm tumor and Bissell group demonstrated that Matrigel™ has important mechanical and chemical properties to illuminate the morphological and functional tumor behavior.[111] However, cancer xenograft would have large variety for tumor size because traditional method is to mix suspended cells with Matrigel™ and then inject into nude mice in vein. Therefore, cancer cells would spread everywhere in nude mice. Once the level of communication between cells is not well, the tumor would not be formed in nude mice. To overcome this large variety and low successful rate, we can make Matrigel™ 3D microenvironment to confine and localize cancer cells at specific location. However, there is no tool to make Matrigel™ 3D microenvironment for xenograft because Matrigel™ is an extremely soft material. Therefore, we can use PASMO to overcome this disadvantage.

We mixed pancreatic tumor cells (AsPC1 Luc cells) with Matrigel™ and filled out the each wells for making microenvironment. Until solidification of Matrigel™, we deform template through injecting air into channel. The Matrigel™ particles will be released from template because extended wells create some space between particles and mold. Therefore, particles in templates can be easily to push and wash out. Particles from PBS are implanted into nude mice. After 7 days, we can observe tumor is formed

in each nude mice. (Figure 23) Compare with control (classical orthotopic model), the successful rate is improved. To consider the volume of tumor, the average of tumor volume is at 12-14mm^3, while the tumor volume in the classical method is from 3.5 to 14.5mm^3. PASMO method can be effectively minimized the variety of cancer xenograft model.

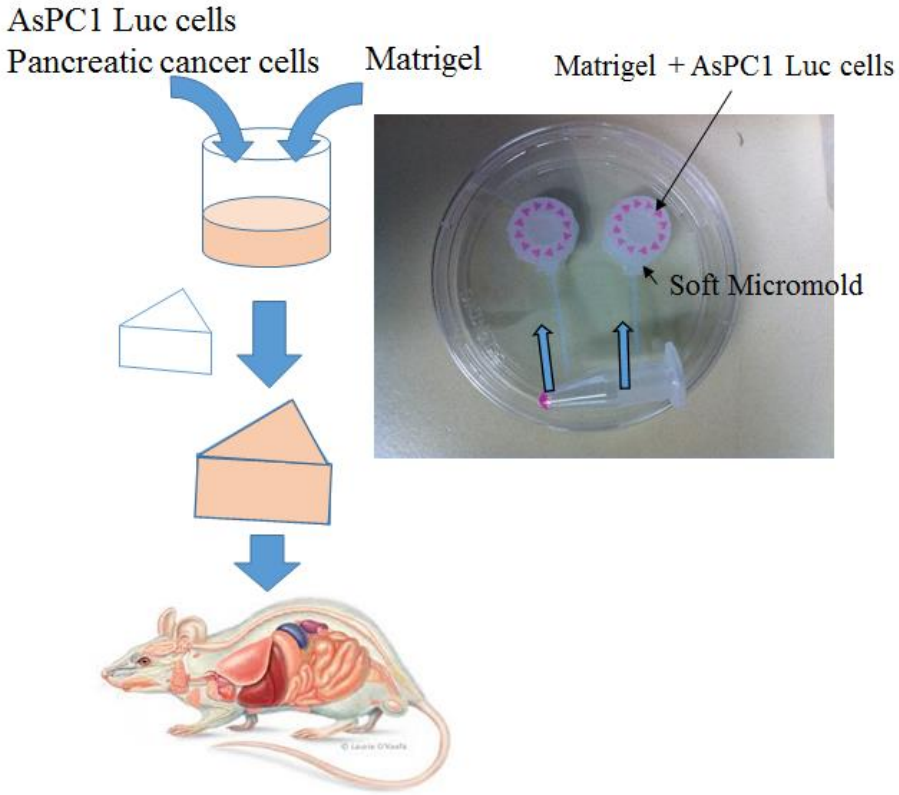

Figure 22 The preparation of xenograft model for AsPC1 Luc cells. AsPC1 Luc cells mixed with Materigel^{TM} and then injected into particles' template of PASMO device for solidification under 37^{o}C. Take off Matrigel^{TM} particles contained AsPC1 Luc cells and implant into nude mice for observing the formation of tumor. The optical image at right hand side is Matrigel^{TM} contained AsPC1 is filled in pneumatically actuated soft micromold device.

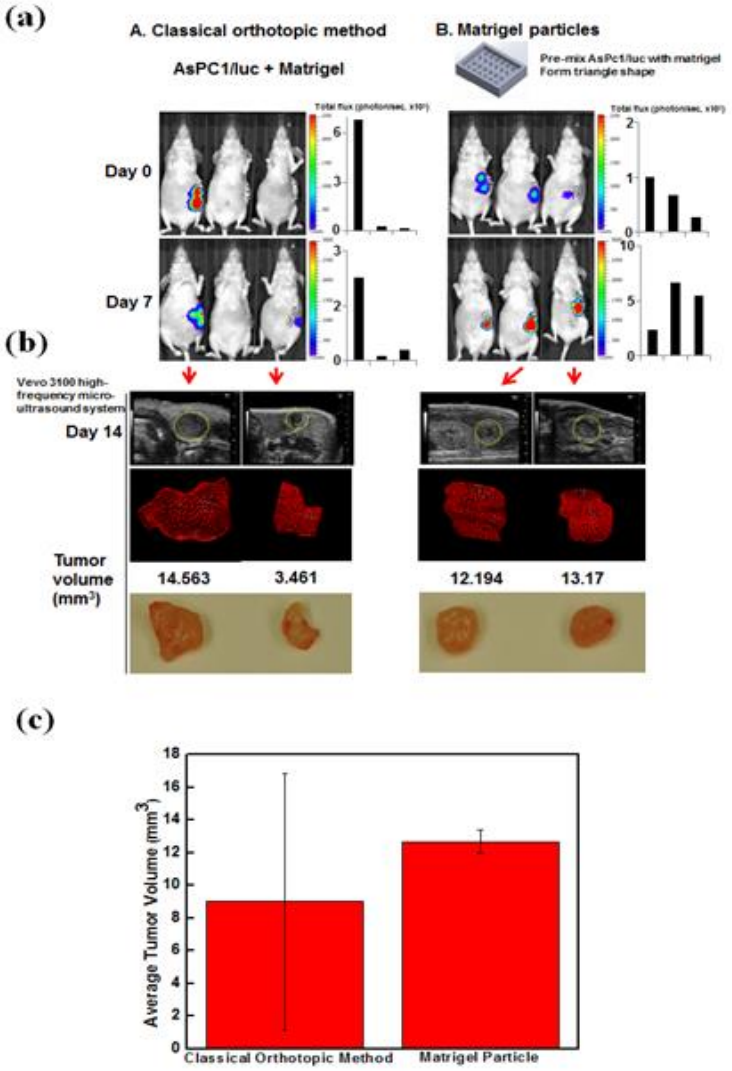

Figure 23 Classical Orthotopic and Matrigel™ particle methods for xenograft model experiment. (a) The bioluminescence images of cancer tissue prepared by the classical orthotopic method and Matrigel particles. Only one nude mice prepared by the classical orthotopic method has response at day zero. All three mice prepare by Matrigel particles have response at day zero. After 7 days, the bioluminescence signal of cancer tissue prepared by classical orthotopic method decreases due to cancer cells spreaded entire body. On the other hand, three mice prepare by Matrigel particles have strong cancer tissue signals. Classical orthotopic method is not able to hold the cells maintaining in the defined volume after injection. Therefore, it might spread closer to skin surface area which caused the signal stronger. However, it might also move to deeper tissue area or diffuse in circulation which caused less signal. PASMO-Matrigel™ already pre-defined the cells within the gel so the signals can be more homogenous. (b) Ultrasonic scanning image of tumor tissue prepared by the classical orthotopic method and Matrigel particles at day 14. Photo images of tumor tissue removed from mice prepared by the classical orthotopic method and Matrigel particles are also shown. (c) The average tumor volumes prepared by the classical orthotopic method and Matrigel particles. Matrigel™ based tumor tissue particles can effectively reduce the fluctuation of tumor volume.

5. ARTIFICIAL ISLETS FOR TYPE I DIABETES TREATMENT

5.1 History of the treatment for type I diabetes

Early stage diabetes patient require strict diet and exercise regimes to control the glucose concentration in blood; if the disease is progressed, patients need to inject insulin. As the stage of diabetes progresses further, diabetic complications, such as heart and blood vessel disease, nerve and eye damages, are often reported. To delay such complications, the glucose concentration in blood should be controlled precisely by multiple insulin injections a day, which has led to varied and often unsatisfying results. For a precise control of the glucose level in blood, numerous insulin delivery methods have been investigated over the past 20 years. The more established delivery methods range from the insulin inhaler,[112] skin patch delivery,[113] insulin pills,[114-115] to the most drastic method of pancreas transplantation.[116] Despite varied success, the aforementioned methods exhibit problems with delivery efficiency,[112-115] as well as potential discomforts. For instance, even the most clinically accepted insulin inhaler (Afreeza marketed by Sanofi) is known to cause dizziness, lung problems and irritation in the back of the mouth.[112] The latest technology in insulin delivery focuses on the encapsulation of beta cells in different media, such as nano-sized pores,[117] polysaccharide (alginate),[118] and polyethylene glycol (PEG).[119] Most study were using PEGDA to generate microenvironment through imprint lithography,[120-123] continuous flow lithography (CFL),[124] and stop flow lithography (SFL)[125] to pattern microparticles and encapsulate beta cells or islet. Cells are mixed with Polyethylene (glycol) Diacrylate (PEGDA) and are dispended to the pattern. However, PEGDA does not have biological

sequence to provide adhesion site for beta cells. Therefore, PEGDA need to modify short peptide sequence, like RGD, IKLLI, IKVAV (laminin sequence) and DGEA (collagen type I sequence) to improve cell viability and reduce apoptosis.[126] Also, the insulin secretion can be also improved by conjugating EphA5-Fc receptor and ephrinA5-Fc ligand.[127] Although the biological function is adjustable, these approaches are just to realize the interaction between peptide sequence and beta cells rather than to mimic the microenvironment for islets and beta cells. Furthermore, the solidification of PEGDA would damage cells because UV-photoinduced cross-linking. Photoinduced cross-linked polymer is polymerized by radical reaction so that UV light would damage cells and then induce cell cytosis and apoptosis during the preparation. While in the preclinical stage of development, nano-pore immune-isolation devices are highly costly to fabricate. On the other hand, PEG reports inflammation and potential immune complications,[128-129] particularly due to the fact that alginate does not originate from the human body.

Collagen is one of the most important extracellular matrix in creating the cellular microenvironment without immnumoresponse, which is similar to the case of islet or beta cells.[130] To culture beta cells or islet in collagen matrix would suppress the dell death and maintain the biological function. Nagata et al. monitored mRNA levels (insulin, glucagon, somatostatin) and secretion levels (HCF, IL-1α and 1β) expressed in collagen matrix to recognize as major insulin secretion and cytotoxic factors for pancreatic beta cells. mRNA levels maintained the same level, while secretion levels does not change after culturing in collagen matrix. It indicates that encapsulated beta cells in collagen microenvironment would not interfere biological function.[131-133]

Currently, several methods to produce collagen microparticles have been reported. For instance, mono-dispersed microfluidic approach is used to create collagen microspheres.[134-140] While the high throughput production is the main advantage, this approach has not been successful in biomedical application because oil phase would inhibit the cellular function in collagen-based microenvironment. Oil-to-water emulsion is an unsolved system to make microsphere. Therefore, oil phase would attach and absorb on the surface of microspheres. Consequently, cellular function would be inhibited. Furthermore, the abnormal cellular function would occur. In addition, the extraction process of collagen microparticles from oil phase would cause contamination and damage of microparticles. Collapsed and merged micropartilces would also undergo during extraction process. On the other hand, the non-uniform collagen microparticles would be happened after extraction process.

Replica molding,[141] Particle Replication In Non-wetting Templates (PRINT^{TM}),[142-143] and bottomless molding technique,[144] are used to produce stable and chemically or physically cross-linked materials, such as alginate or collagen. Gelated collagen microparticles are extracted from the templates manually pushing molds. These approaches are the only technique to produce collagen particles, however it has very low throughput and the extraction of particles without damage is still challenging due to the inherent softness of collagen. Squeezing the micro-mold is the most traditional method of extraction but the inhomogeneous extraction force easily damages soft collagen microparticles. In conclusion, no technique is presently available to synthesize a large number of collagen microparticles, economically, reliably and reproducibly.

In this study, we developed pneumatic actuator to gently extract collagen microparticles. This pneumatic actuator is composed by three sections shown in Figure 24a. These three sections are particles' template, air channel, and resistance layer. The working strategy of cPASMO device can be classified as four steps to release collagen microparticles. First of all, the collagen solution is filled into each wells located on particles' template and incubate it at 37^{o}C for 30 min for solidification. Second, air is injected into air channel to increase the inner pressure for deformation. According to the asymmetric mechanical properties of cPASMO device, the deformation of particles' template is more obvious than resistance layer. Therefore, the gap would generate between mold and collagen microparticles. Thirdly, buffer or culture media can diffuse into the gaps to float and push collagen microparticles out without damage. Finally, collagen microparticles can be collected from buffer or culture media for monitoring the cellular response. Herein, we use cPASMO device to produce artificial islet through encapsulating beta cells and monitor the concentration of insulin secreted from encapsulated beta cells.

5.2 Fabrication of circular pneumatic actuated soft micromold

The circular Pneumatic Actuated Soft Microfmold (cPASMO), shown in Figure 24a is constructed by three layers. Top layer is the particles' template, which is used to generate collagen microparticles and middle layer is air channel for creating the pneumatic actuation. This actuation can deform particles' template in order to generate gaps for releasing collagen microparticles. Moreover, pneumatic actuation is controllable through varying the injected volume and injected rate of air so that collagen

microparticles can be extracted gently. The bottom layer, third layer, performs stronger mechanical property and constructs a resistance for deforming from bottom side. On the other hand, the bottom resistance distributes and transports pneumatic force to particles' template for deformation. Figure 24b to 24d presents the process to prepare particles' template, air channel and resistance layer, respectively. Particles' template and air channel layer of cPASMO device are fabricated by Ecoflex-30®, while the resistance layer is composed by Ecoflex-30®-cloth composite, which has stronger mechanical properties. Each layer is duplicated from 3D-printed mold, which is printed from EnvisionTec. The uncured Ecoflex-30® is poured in 3D-printed mold for making particles' template, air channel and resistance layer, respectively. Then, the bonding between these three layers is operated by Ecoflex-30® and the curing time is 4 hours at room temperature.

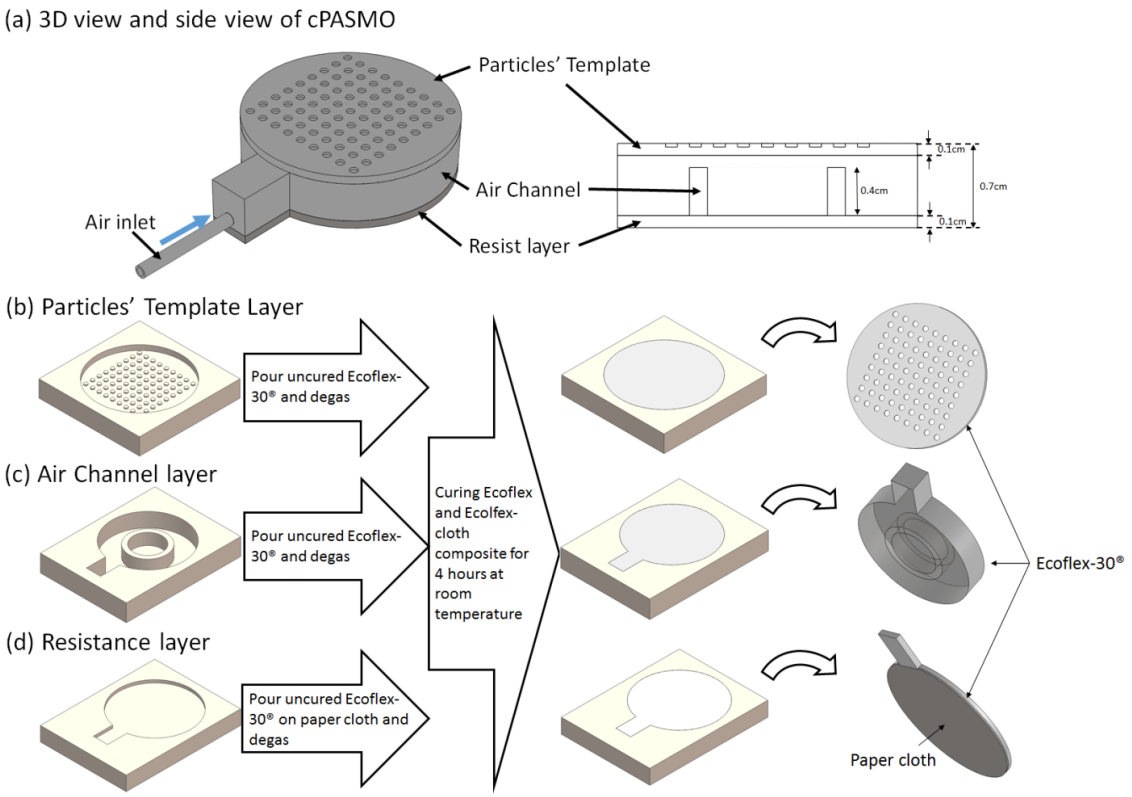

Figure 24 Schematic diagram of circular pneumatic actuated soft micromolds (cPASMO) device (a) 3D and top view of circular PASMO device, which is composed by three layers, template layer, channel part and resist layer. Molds is printed through 3D printer. (b-d) The master mold of particles' template, air channel and resistance are prepared from 3D printer, respectively. Pour uncured Ecoflex-30® into each mold and cure it for 4 hours at room temperature. After solidification, the parts of cPASMO can be peeled from mold. Uncure Ecoflex-30® is used as glue to bond these layers for 4 hours.

5.3 Preparation of artificial islet for beta-cell encapsulation

Collagen, alginate, and polyethylene glycol diacrylate (PEGDA) are the target matrixes for encapsulating beta cells and producing artificial islet. Collagen microparticles are fabricated from collagen type I solution extracted from rat tail and the final concentration for cell encapsulation is 3.5mg/mL;[145] Alginate microparticles are constructed by 1% sodium alginate extracted from brown algae and the cross-linking of alginate is triggered by 1M calcium chloride. The cross-linking of alginate is 30 seconds;[124] PEGDA microparticles are formed by polyethylene glycol diacrylate and its average molecular weight is 575Da.[146] The mechanism of cross-linking of PEGDA is photo-polymerization. Thus, 3% of photoinitiator (2,2-Dimethoxy-2-phenylacetophenone) is prepared for the cross-linking of PEGDA microparticles. The duration of cross-linking of PEGDA is 30 seconds.

For cell encapsulation inside collagen, alginate and PEGDA microparticles, beta cells are mix with 3.5 mg/mL collagen solution and PEGDA solution, respectively. Then, these mixtures are dispensed into particles' template of cPASMO device and trigger cross-linking for each material under proper conditions. Solidified microparticles are released from the deformed particles' template of cPASMO device into RPMI-1640 culture media. There microparticles encapsulated beta cells are cultured in a humidified incubator (5% CO_2 and 95% air condition) at 37^{o}C for more than 14 days and monitor the insulin secretion. The concentration of beta cells for all experiments is set to 2×10^7 cell/mL. The size for microparticles is 500 μm and 1000 μm in diameter and the thickness is 300μm. On the other hand, the average of cell number of 500 μm and 1000

μm microparticles are 1180 and 4710, respectively. The cPASMO device is autoclaved at 131^{o}C for sterilizing.

Figure 25a presents the schematic diagram of top view of cPASMO. The solid line is the boundary of cPASMO device and the dash line is the pattern of air channel, which is designed as circular shape. The circular design of air channel expands the particles' template radially when pressurized. This radial expansion not only can create the gap between mold and collagen micro-disk but also can reduce the depth of particles' mold to extract collagen particles.

The dimension and the position of the air channel crucially determine how the cPASMO device deforms after increasing the inner pressure. The parameters W, D_i, and D_o stand for the width of air channel, inner diameter and outer diameter, respectively and we used W-D_i-D_o to describe the dimension of cPASMO device. For example, 0.3-1.7-2.5 indicates that the width of channel, location of air channel, and diameter of cPASMO are 0.3, 1.7, and 2.5cm, respectively. Figure 25b presents the relationship between the percentage of expanded area and inner pressure. The expanded area increases as a function of inner pressure. The larger the inner pressure we generate, the wider the expanded area of the cPASMO device are. As a result, the saturated expanded area is 5 times wider than original size. To simply the name of cPASMO with different designs, 0.3-1.7-2.5 is called cPASMO_1.7.

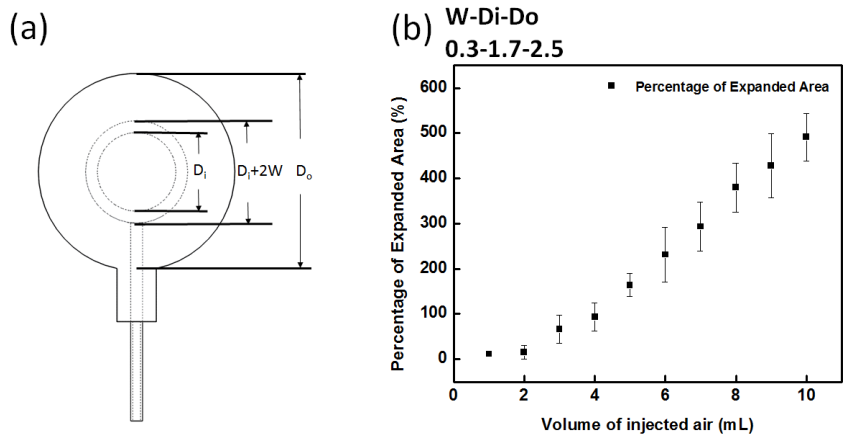

Figure 25 Circular PASMO deformation at different injected volume of air (a) schematic diagram for cPASMO device from top view (b) the expanded area of particles layer of cPASMO.

Herein, we produce four types of cPASMO devices with different positions of air channel, which locates at 1.0 (cPASMO_1.0), 1.4 (cPASMO_1.4), 1.7 (cPASMO_1.7), and 2.0cm (cPASMO_2.0), respectively, using FE. Figure 26 presents the deformed configurations for these four cPASMO devices from the simulation. This table arranges side view and top view of deformed cPASMO. The most important characterization is that the morphology of expansion of particles' template is highly related with the position of air channel. As in the previous mechanism of releasing particles, generating a wider gap between the mold and collagen particles can help releasing of collagen microparticles. Moreover, releasing percentage of collagen microparticles is another important aspect for producing collagen particles through cPAMSO in order to increase the efficiency. Therefore, the optimized cPASMO needs to perform wider generated gap and higher releasing rate of collagen microparticles after pneumatic deformation.

The generated gap is determined by expanded area of each particles' wells. Figure 3 presents the expanded area after pneumatic deformation. According to the different

expanded level of deformation at different area, particles' wells are classified as seven areas, which indicate area 1 to area 7 from the outer to inner regions shown in Figure 27a. Figure 27b to 27e presents the distribution of expanded areas from area 1 to area 7 in cPASMO_1.0 to cPASMO_2.0. The maximum expanded area is located at channel's position because of larger deformation generated from the center of air channel. For example, cPASMO_1.0 performs a maximum deformation at area 7, which indicates the position of channel. The further location from the air channel decreases the deformation level of particles' well because the pneumatic force cannot propagate through the whole cPASMO device. It demonstrates that the outer region, area 1 to area 3 cannot properly generate a gap between mold and collagen microparticles. cPASMO_2.0 is designed as improving the amount of expanded wells and the design of cPASMO_1.4 is to locate the air channel in the middle region, which is close to area 6. This location contributes wider distribution of expanded wells and the range of expanded area is 1.1, 2.8, 7.2, 11.1, 10.9, 9.5, and 3.9 mm^2 from area 1 to area 7, respectively. Figure 3c shows the distribution of expanded area of each particles' well on cPASMO_1.4. However, the maximum deformed particles' wells is not located at the air channel position. The position of air channel for cPASMO_1.0 is located at central region so that the lateral resistance is higher than the vertical resistance due to the thickness of Ecoflex-30®. The lateral thickness is 1.5 cm, while the vertical thickness is 2.0mm. Therefore, the pneumatic force contributes to the vertical deformation more than the lateral deformation in cPASMO_1.0 design. Once the lateral resistance decreases with decreasing the lateral thickness, like cPASMO_1.4, the pneumatic force would contribute to both lateral and

vertical deformations. This deformation arrangement helps improving the expansion at wider region. Figure 27d shows the distribution of deformed particles' wells for cPASMO_1.7. cPASMO_1.7 shifts the location of air channel to 1.7cm and the thickness reduces from 5.5cm (cPASMO_1.4) to 4cm (cPASMO_1.7). The expanded areas are 1.8, 6.0, 11.9, 10.3, 10.5, 7.2, and 2.5mm^2 from area 1 to area 7, respectively and the maximum expanded area also follows the position of air channel to shift to area 3. The deformation of particles' well and expanded area of each region on cPASMO_1.7 is similar as cPASMO_1.4 so that cPASMO_1.7 can also contribute radial deformation. However, if the position of air channel moves further to 2.0cm called cPASMO_2.0, the lateral deformation would more obvious than the vertical deformation because of low lateral resistance. The lateral thickness reduces from 5.5mm (cPASMO_1.4) to 2.5mm and this position is close to the vertical thickness, 2.0mm, so that the lateral resistance is approximately equal to the vertical resistance. The distribution of expanded area shifts to outer region, area 3 and the expanded areas for each area are 1.1, 3.0, 5.0, 3.7, 4.3, 1.7, and 0.8 mm^2 from area 1 to area 7, respectively. The pneumatic force generated from air channel for cPASMO_2.0 cannot propagate and contribute to central region (area 6 and area 7) so that the expanded area of particles' wells cannot properly produce gaps between the collagen microparticles and mold. Figure 28 presents the quantified results for serial cPASMO designs, cPASMO_1.0 cPASMO_1.4, cPASMO_1.7, and cPASMO_2.0. The amount of deformed particles' wells and the releasing rate of collagen microparticles are important characterization of cPASMO device. We define the amount of deformed particles' wells as follows:

$$Amount\ of\ deformed\ wells\ (\%) = \frac{\#\ of\ deformed\ wells}{total\ wells} \quad (1)$$

Figure 28a summarizes the amount of maximum deformations in wells based on the location of air channel. The expanded particles' wells are located at areas 5 to 7 but the particles' wells posited at area 1 to 4 experience relatively small deformations. The amount of areas that can undergo significant deformations in wells for cPASMO_1.0 is around 70.4%. Even through cPASMO_1.4, cPASMO_1.7, and cPASMO_2.0 can undergo significant deformations, the amount of deformed areas for cPASMO_2.0 is around 64.2% due to an undeformed region at the center of the device. From the contour plot of cPASMO device in Figure 27, cPASMO_2.0 shows relatively small deformations at the center of the device after actuation, indicated by blue region. On the other hand, cPASMO_1.4 and cPASMO_1.7 can trigger over 95% of particles' wells' deformation. Moreover, the average expanded area of cPASMO_1.4 and cPASMO_1.7 can approach 6.64 and 6.44mm^2, respectively. Compared to the maximum expanded area of particles' wells, cPASMO_1.4 and cPASMO_1.7 can create 11.9 and 11.1mm^2. Figure 28b demonstrates the comparison of expanded areas between these four cPASMO devices. Creating larger gap and generating larger mold expansion can enhance the releasing rate of collagen micro-disks without damaging the particles. Figure 28c illustrates the releasing rate of collagen micro-disks in these four cPASMO devices. The releasing rate

of collagen micro-disks is calculated by the ratio of number of released particles and total wells. The formula is shown as below:

$$Releasing\ collagen\ microdisk\ (\%) = \frac{\#\ of\ released\ particles}{total\ wells} \qquad (2)$$

The design of cPASMO_1.0 and cPAMSO_2.0 are evident that the releasing rates are 54.1% and 50.5%, respectively, while cPASMO_1.4 and cPASMO_1.7 show the releasing rates of 95.5% and 90.2% respectively. The results of releasing rate match the deformation of cPASMO device. Higher level of expansion and larger amount of deformed particles' wells of cPASMO lead to higher release of undamaged collagen micro-disks cPASMO. The optimized designs of cPASMO device are cPASMO_1.4 and cPASMO_1.7, whose location of the air channel is in the middle of cPASMO device. This design can generate proper magnitude of mold expansion and larger amount of deformed particles' wells.

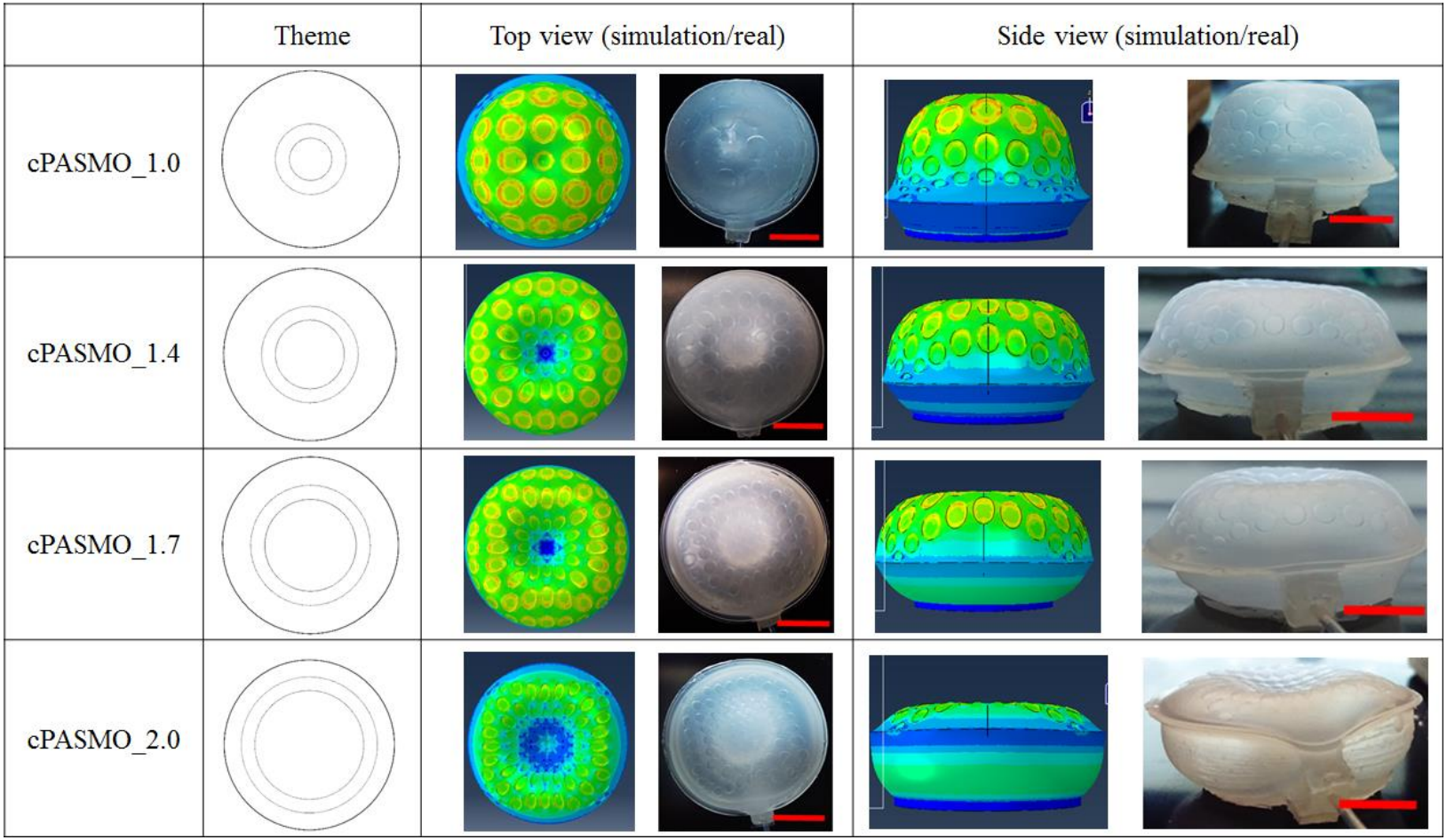

Figure 26 Deformation and actuation of cPASMO device for different dimensions. cPASMO is classified as four group based on the position of air channel, cPASMO_1.0, cPAMSO_1.4, cPASMO_1.7, and cPASMO_2.0, respectively and the unit of number is centimeter. In this figure, we present the simulated and optical image for different designs after actuation. And the pictures are from top and side views for presenting the deformation for each dimensions. The diameter of cPASMO device is 2.5cm. (Scale bar: 2cm)

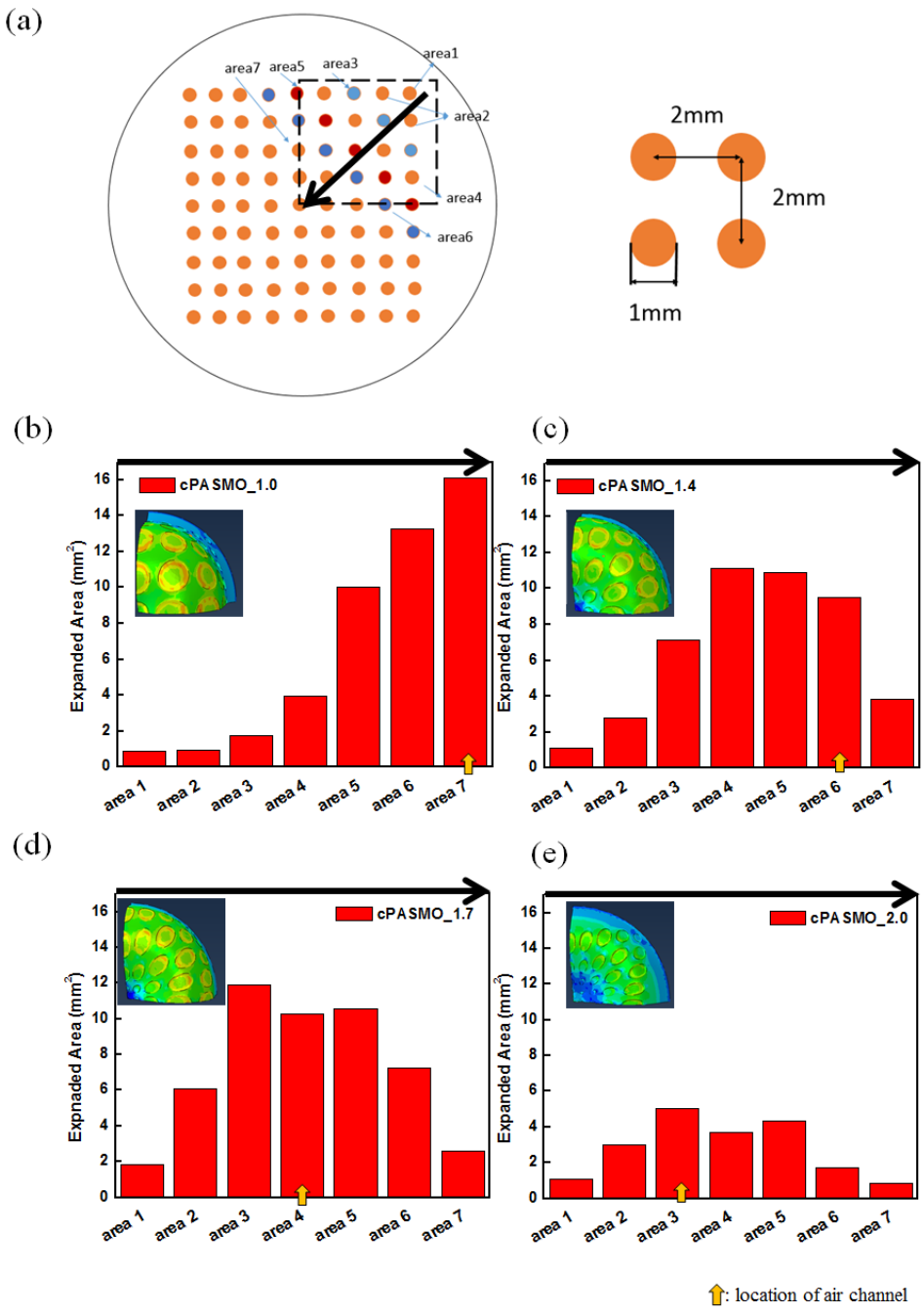

Figure 27 Expanded area of cPASMO device from seven areas. (a) Schematic diagram of micro-disks' mold of cPASMO device and we distinguished as seven areas, area 1 to area 7 from outer to inner, respectively. (b) cPASMO_1.0 presents the expanded area varied from area 1 to area 7. The position of air channel is located at area 7. (c) cPASMO_1.4 presents the expanded area varied from area 1 to area 7. The position of air channel is located at area 6. (d) cPASMO_1.7 presents the expanded area varied from area 1 to area 7. The position of air channel is located at area 4. (e) cPASMO_2.0 presents the expanded area varied from area 1 to area 7. The position of air channel is located at area 3.

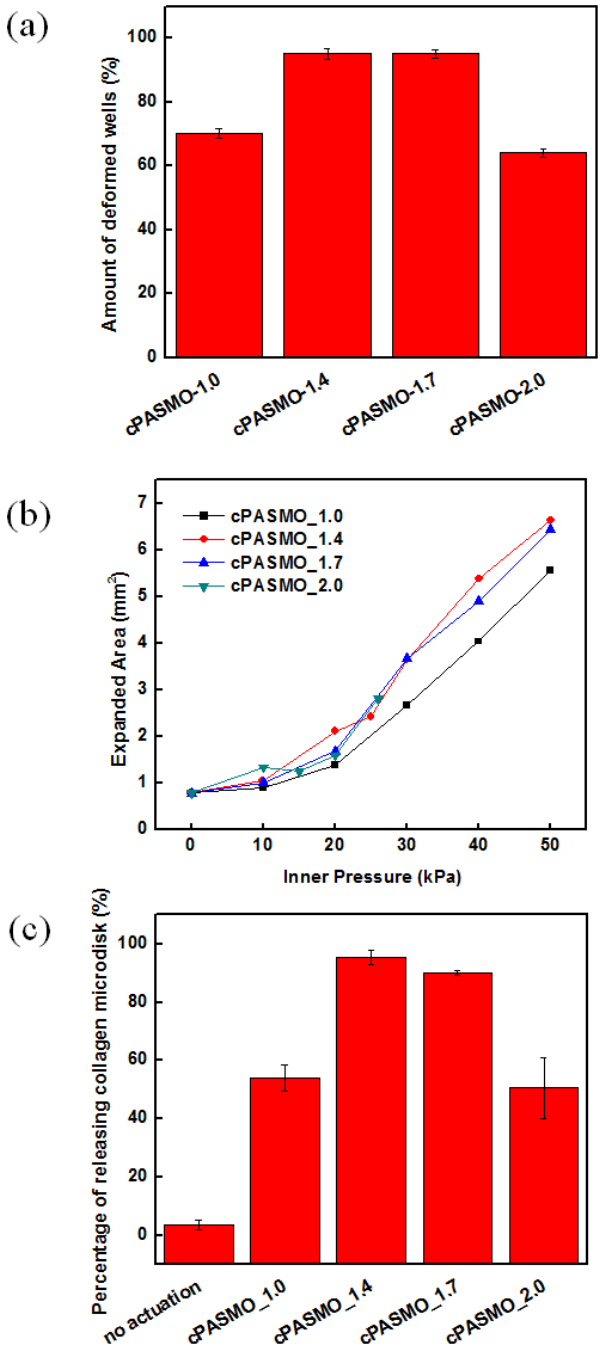

Figure 28 Comparison and optimization of cPASMO within different dimensions. (a) Amount of deformed wells, which is defined as the ratio between the number of expanded wells and total wells. The highest percentage of expanded wells is cPASMO_1.4 and cPAMSO_1.7 (b) Comparison of expanded area between different dimensions and their expanded areas are proportional to the inner pressure. cPASMO_1.4 and cPAMSO_1.7 performed highest expanded area. (c) Comparison of releasing rate of collagen micro-disk of cPASMO device and the highest releasing rate is cPASMO_1.4 and cPASMO_1.7.

Figure 29 shows the glucose response for collagen based artificial islets under four-step cycle. The inserted wells are placed on each well of 24 well plate for holding suspended artificial islets and this inserted wells have porous to allow the diffusion of glucose and secreted insulin. As a result, the secreted insulin level can be monitored from collected culture media outside inserted wells. The first step is the control group, which includes culture media contained 25mM glucose only and the concentration of secreted insulin is 0.251ng/mL. Secondly, 3~4 artificial islets are placed into inserted wells and the culture media includes 25mM glucose. After 24 hours culturing, the concentration of secreted insulin can approach 2.382ng/mL. Later, the culture media is replaced to the culture media lacking of glucose for monitoring the concentration of secreted insulin from artificial islet after 45 min incubation. As a result, the concentration of secreted insulin decreases to the background value. Finally, the glucose is added in culture media again and the concentration of glucose is 25mM. After 45 min incubation, the secreted insulin level rises and achieves detectable range. This result demonstrates that these articles islets not only can survive in collagen micro-disk but also can maintain their biological function, like sensing glucose from surrounding and secreting insulin after glucose stimulation.

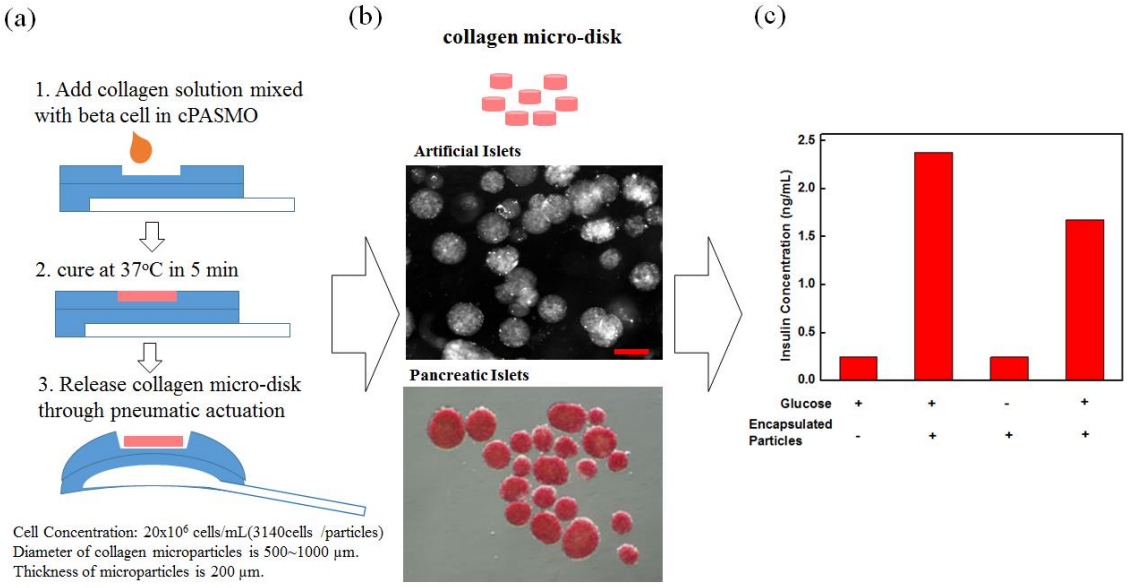

Figure 29 Glucose response of encapsulated beta-cells in collagen disk for secreting insulin. (a) procedure of encapsulating beta cells in collagen disk. (b) Microscopic image of collagen disk encapsulated beta cells and the cell concentration is 3140 cells per collagen disk (c) Insulin response under four continuous steps. First step is that culture media contains glucose only. Second step is to add the collagen disks containing beta cells into glucose-culture media. The third step is to replace the culture media, which does not contain glucose. The fourth step is for changing back the culture media contained glucose

Figure 30a demonstrates the material effect for encapsulating beta cells. We encapsulate beta cells in PEGDA and collagen. The insulin secretion level for PEGDA is much less than the one from the collagen-based micro-disks and suspended beta cells. This indicates that the cellular function of beta cells already missed after encapsulation in PEGDA. On the other hand, the encapsulated beta cells can maintain their cellular function, which is related with the interaction between matrix and cells.[125-126,149] For example, RGD functionalized PEGDA can effectively revive encapsulated beta cells for sensing glucose and releasing insulin. Moreover, encapsulated beta cells in collagen micro-disk perform higher insulin secretion level than suspended beta cells. It proves that the insulin secretion depends on the distance between cells for signal transduction.

Collagen micro-disk provides an approach to forming cluster for beta cells. Figure S1 presents the glucose response under four-step cycle test for collagen-based micro-disk. This result also demonstrates that the artificial islet can respond to glucose from surrounding. Additionally, the secretion of insulin for artificial islets increases as a function of glucose concentration. Figure 5b presents that artificial islets are in culture media with different concentrations of glucose (2mM, 15mM, and 30mM). Higher insulin concentration leads to higher glucose concentration. Moreover, in each concentration, artificial islets can secret insulin 3~6 times higher than the suspended one. The reason is that the secretion of insulin is determined by the signal communication between each beta cell. If the distance between each beta cell is short enough, the triggered signal will be transported to more cells. Moreover, we consider different dimensions of artificial islets, which is 500μm and 1000μm, respectively. A smaller artificial islet can secrete higher insulin even when the number of cells is half of the one in the larger artificial islets. One reason for higher insulin secretion from smaller islet is due to the diffusion behavior. Smaller collagen microparitcles have less diffusion resistance than the larger ones so that smaller microparticles would be easy to sense and respond to the change from surroundings. Another reason is that the distance between beta cells. The signal transduction between beta cells is proportional to the insulin secretion. A closer distance in the micro-disk beta cells produces higher insulin beta cells secretion. As a result, smaller artificial islet would secrete higher concentration of insulin than the larger one. cPASMO offers a promising approach to fabricate collagen-based micro-disk as an artificial islet.

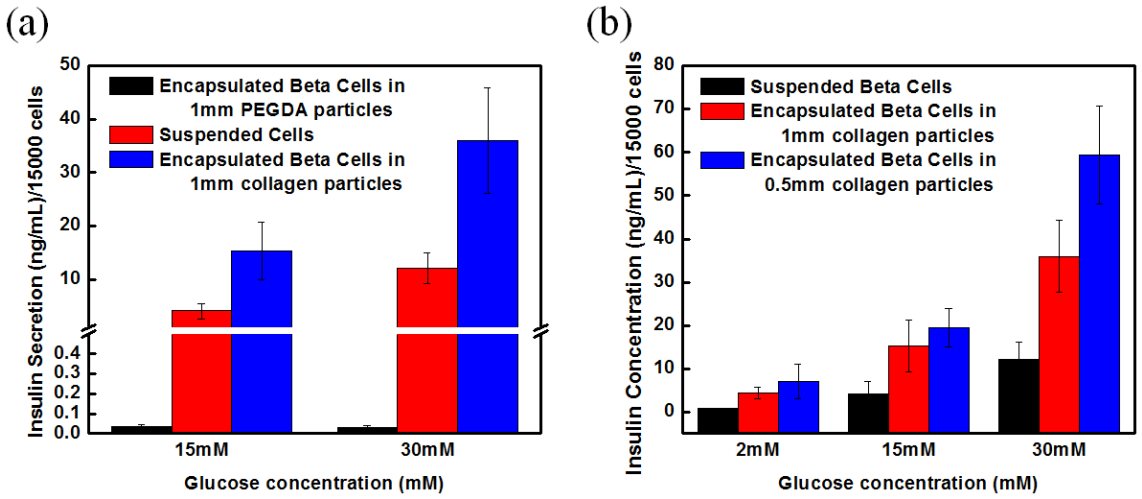

Figure 30 The performance for secreting insulin at different concentrations of glucose (a) comparison of secreting insulin between suspended cells and encapsulated cells in collagen disks and PEGDA disks. The glucose concentration in culture media is 15mM and 30mM, respectively. (b) comparison of secreting insulin in different size of collagen disks. We produce collagen disks within 0.5mm and 1mm in diameter and suspended them in culture media within different concentrations of glucose, 2mM, 15mM, and 30mM.

5.4 Artificial islet implantation

Type I diabetes mellitus is a group of metabolic diseases in which the insulin secretion is abnormal due to losing function of pancreatic islet, especially beta cells.[150] The most reliable clinical therapy is islet transplantation, which is called "Edmonton protocol".[151] The major issue to impede this surgery is the immunoresponse. The isolated islet would induce the immunoresponse because of transplantation immunity.[152] Therefore, permanent immunosuppresant would introduce to provide immnuo-tolerance after transplantation. For example, tacrolimus and silolimus are the well-known immunosuppressants for islet transplantation, however, they impair the islet viability and graft function.[153-154] beta cells encapsulated in collagen microenvironment can reduce the immune-response because collagen microenvironment can be used as barrier to avoid triggering immune reaction and prevent the adhesion of immune cells.[155-156] The second

issue for islet transplantation is the surgery method. Based on the position, islet transplantation would be classified as intravascular and extravascular types. An intravascular is directly transplant beta-cell microenvironment into the host artery and vein.[157] The beta-cell microenvironment would attach onto wall of blood vessel. Once blood flows through this microenvironment, the oxygen and nutrient would be delivered and the water would be taken away. However, the severe problem for intravascular transplantation is that the blood clots would be generated in blood vessel. The ideal transplantation site for encapsulated beta cells is extravascular, especially intrahepatic transplantation. However, intrahepatic transplantation would induce instant blood-mediated inflammatory reaction (IBMIR, a rapid process for forming thrombus.[158] To improve and reduce IMBIR after transplanting artificial islets, muscle and subcutaneous tissue can be considered as the best positions.

Figure 31a is the process to prepare the sample for islet transplantation. We prepare 300 collagen-based microparticles contained beta cells, and then transferred them into big mold in which the size is 3mm × 3mm × 2mm (height). Collagen precursor is added into millimold in order to aggregate 300 collagen microparticles as the clusters. We continue with a subcutaneous injection to transplant this cluster into mice. Figure 31b shows the testing on mice to check the angiogenesis. The white area is the cluster of collagen microparticles and we found the blood vessels (red line) are formed around the cluster of collagen microparticles. Moreover, by homogenizing the cluster, the insulin secretion can be monitored. We also implant artificial islet clusters at two locations. After three weeks, the blood vessels can form around these two clusters and there are

blood vessels formed between them, as shown in Figure 32. On the other hand, the forming of blood vessel can be used to regulate blood glucose level and the connection between tow clusters can improve the efficiency for regulating sugar level in blood. The concentration of insulin from this tissue is 163.6pmol/L, which is close to normal condition. Artificial islets can potentially compensate the insufficient insulin for type I diabetes patients.

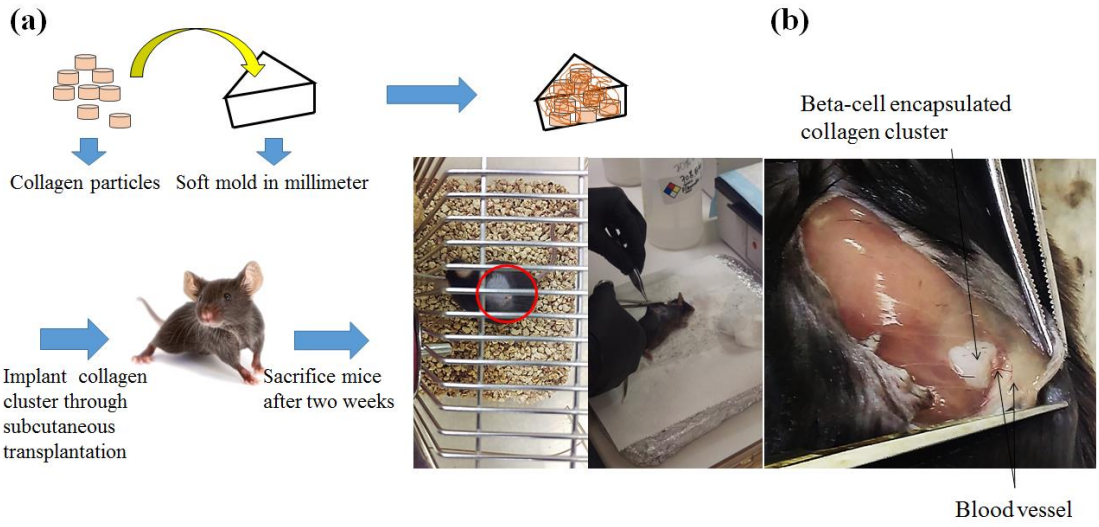

Figure 31 The process for artificial islet implantation-one location after one week (a) Collagen microparticles contained beta cells formed through cPASMO device and 300 microparticles are placed into larger PASMO wells. Another collagen solution is poured into wells for clustering these 300 microparticles. Finally, this cluster is implant into mice under skin and sacrifice mice after one week. (b) Blood vessel is formed around the implanted artificial islet and the concentration of secreted insulin is approach the normal level.

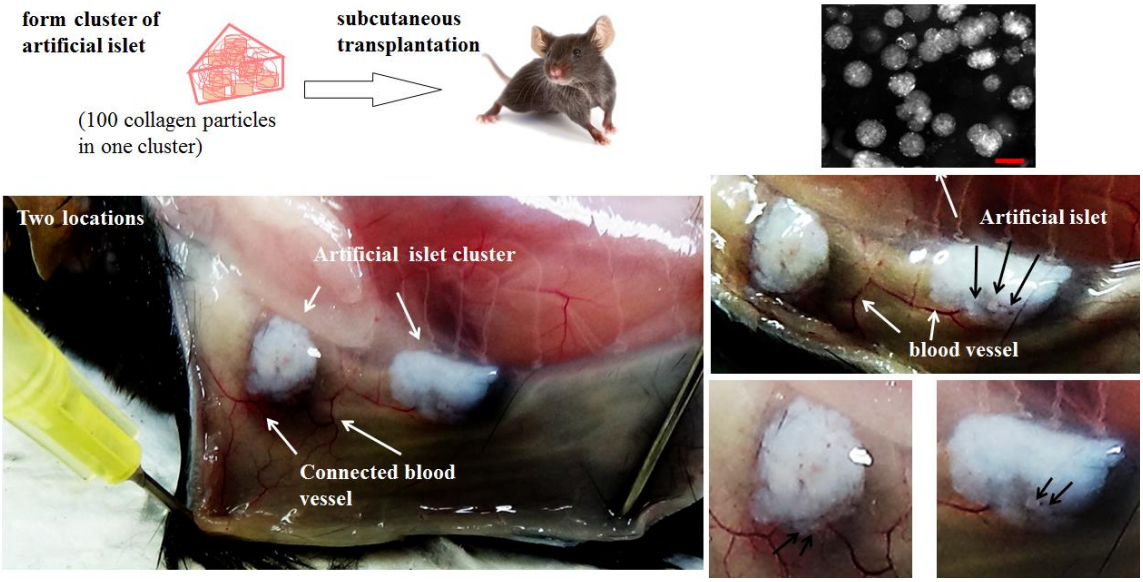

Figure 32 The process for artificial islet implantation-two locations after three weeks. Collagen microparticles contained beta cells formed through cPASMO device and 100 microparticles are placed into larger PASMO wells. Another collagen solution is poured into wells for clustering these 100 microparticles. Finally, this cluster is implant into mice under skin and sacrifice mice after one week. After 3 weeks and sacrificing mice, blood vessel is also formed around the implanted artificial islet and there is connection between two implanted beta cells clusters.

6. SUMMARY

In this dissertation, two different designs of pneumatic actuated soft micromold (PASMO) are used to generate collagen microstructure within different dimensions and different morphologies. An overview of design of PASMO device is given as an introduction to PASMO fabrication. Then two different designs of PASMO is discussed in detail for their biological application.

Pneumatic actuated soft micromold (PASMO) is constructed by three layers, particles' template, air channel and resistance sheet, from top to bottom, respectively. Particles' templates and air channel are built by Ecoflex® and the resistance sheet is composed by Ecoflex-30®-cloth. Ecoflex-30® and Ecoflex-30®-cloth composite, which perform soft and stiff mechanical properties, respectively. Therefore, the expansion of particles' template generates through the actuation of PASMO after injecting air. This expansion allow liquid to diffuse into wells of particles' template and help the extraction of collagen particles. The working strategy of PASMO can be classified into four steps: filling collagen solution mixed with cells, solidification of collagen solution, and expansion of particles' template after pneumatic actuation, and extraction of collagen particles. The collagen particles can be easily duplicated from particles' template and these particles perform highly stability over 60 days. The corresponding collagen fibulas density has also been found to be comparable to the one in real tissue environment. The high fiber density allows for collagen microstructures to be implanted through syringe and remain intact.

The deformation of PASMO relies on the design of air channel. In this dissertation, we present two different channel designs, straight and circular channel to generate different deformation. PASMO within straight channel can perform the one-dimensional elongation of particles' template in order to extract collagen particles. To demonstrate the merits of using PASMO contained straight channel for creating cellular environment, millimeter scale of collagen particles can be duplicated without any damage during extraction.

MDA-MB-231-GFP cells are encapsulated in these collagen particles in millimeter by PASMO devices as modular microenvironment. The cells proliferate continuously more than 14 days in this microenvironment. Deformations and contractions of collagen particles are simultaneously observed during this period, with cancer cells identified as the primary cause of contraction. Collagen particles can also monitor in anti-cancer drug response based on the contraction from cells. Moreover, Matrigel^{TM} particles produced by PASMO devices can effectively localize the tumor cells at specific location in order to develop tumor tissue. Moreover, the tumor volume developed by Matrigel^{TM} particles is more uniform than those made by the classical orthotopic method. These results indicate that collagen and Matrigel^{TM} microstructures produced by PASMO devices possess the potential to improve cancer research.

Circular channel is another design for PASMO device and the deformation of PASMO device belongs to two-dimensional expansion. Therefore, circular channel design of PASMO can be used to fabricate smaller or more complicated structure for creating collagen microenvironment. Additionally, Circular design can perform larger

level of expansion. The expanded area created from circular design presents 6 fold wider than the expanded area from straight design. Larger expansion can allow more buffer or culture media to diffuse into the expanded area for floating and extracting collagen microenvironment from PASMO device. Beta cells encapsulated in collagen micro-disks can maintain their basic cellular function and these cells in micro-disk can proliferate continuously more than 14 days. Insulin secretion of artificial islet is observed during the four-step cycle. When glucose presents but artificial islet is absent in culture media, there is no insulin detected in culture media. Once artificial islets are added into the solution contained glucose, the insulin can be monitored in culture media. Then, artificial islets are shifted to the culture media lacking of glucose and the level of secreted insulin would return to zero. Finally, these artificial islets and glucose are present in culture media and the secreted insulin can be measured again. According to this cyclic test, we can observe artificial islets can maintain and regular their cellular function based on the changing of environment.

PASMO and cPASMO devices provide a controllable process to release microparticles gently through adjusting the inner pressure so that cPASMO can apply in producing extremely soft and fragile material, like collagen. In this dissertation, collagen 3D microenvironment can be used observed the cellular response based different stimuli from surrounding. Moreover, the confinement of cells at adjusted location not only can improve the cellular response but also can reduce the variety of animal experiment. Except collagen, we can also use PASMO device to manufacture different materials,

especially for extremely soft biomaterial, like alginate, agarose, to create cellular microenvironment within specific shape.

PASMO devices are made of silicone rubber that has elastic responses under large deformations and are durable for multiple cycles of deformations. We used a single PASMO device more than hundred times by pressurizing and depressurizing them, we did not notice any permanent deformations or damages in the devices. Based on this observation, we can conclude that PASMO devices are re-usable for several hundred cycles.

Additionally, soft robotics technology will be more and more demanded in biomedical fields in the future. As proven in this dissertation, soft robotics is superior to handle soft and fragile materials such as cells, tissues, organs due to soft nature. Handling such fragile biostructures is critical process in biomedical fields for general surgery, laparoscopic surgery, and endoscopy and implantation applications.

REFERENCES

1. Harry Eagle, and George E. Foley, *Cancer Res*., 1958, **18**, 1017-1025.
2. Erich Hirschberg, *Cancer Res*., 1958, **18**, 869-878.
3. Robert H. Shoemaker, Mary K. Wolpert-DeFilippes, David H. Kern, Michael M. Lieber, Robert W. Makuch, Nannette R. Melnick, William T. Miller, Sydney E. Salmon, Richard M. Simon, John M. Venditti, and Daniel D. Von Hoff, *Cancer Res*., 1985, **45**, 2145-2153.
4. H H Fiebig, A Maier, and A M Burger, *Eur. J. Cancer.*, 2004, **40**, 802-820.
5. Francesco Pampaloni, Emmanuel G. Reynaud, and Ernst H. K. Stelzer, *Nature Reviews Molecular Cell Biology.*, 2007, **8**, 839-845.
6. Keiran S. M. Smalley, Mercedes Lioni, and Meenhard Herlyn, *In Vitro Cell Dev. Biol. Anim.*, 2006, **42**, 242-247.
7. Allison L. Berrier, and Kenneth M. Yamada, *J. Cell Physiol.*, 2007, **213**, 565-573.
8. Erin L. Baker, Roger T. Bonnecaze, and Muhammad H. Zaman, *Biophysical Journal.*, 2009, **97**, 1013-1021.
9. Mark W. Tibbitt, and Kristi S. Anseth, *Biotechnol Bioeng.* 2009;**103**(4):655-663
10. J.E. Barralet, L. Wang, M. Lawson, J.T. Triffitt, P.R. Cooper, and R.M. Shelton, *J. Mater. Sci. Mater. Med.*, 2005, **16**, 515-519.
11. Frederick Grinnell, *Trends Cell Biol.*, 2003, **13**, 264-269.
12. Brian Fallica, Joseph S. Maffei, Shaun Villa, Guy Makin, and Muhammad Zaman, *PLoS One.*, 2012, **7**, e48024.

13. Lisa A. Gurski, Nicholas J. Petrelli, Xinqiao Jia, and Mary C. Farach-Carson, *Assay Drug Dev. Technol.*, 2014, **12**, 207-218.

14. Anna C. Luca, Sabrina Mersch, René Deenen, Stephan Schmidt, Isabelle Messner, Karl-Ludwig Schäfer, Stephan E. Baldus, Wolfgang Huckenbeck, Roland P. Piekorz, Wolfram T. Knoefel, Andreas Krieg, and Nikolas H. Stoecklein, *PLoS One.*, 2013, **8**(3), e59689.

15. Kenny Chitcholtan, Peter H Sykes, and John J Evans, *J. Transl. Med.*, 2012, **10**, 38.

16. Anna Birgersdotter, Rickard Sandberg, and Ingemar Ernberg, *Semin. Cancer Biol.*, 2005, **15**, 405-412.

17. Emmanuel Garcion, Aida Halilagic, Andreas Faissner, and Charles ffrench-Constant, *Development.*, 2004, **131**, 3423-3432.

18. Yukiko M. Yamashita, Margaret T. Fuller, and D. Leanne Jones, *J. Cell Sci.*, 2005, **118**, 665-672.

19. Fei Wang, Valerie M. Weaver, Ole W. Petersen, Carolyn A. Larabell, Shoukat Dedhar, Per Briand, Ruth Lupu, and Mina J. Bissell, *Proc. Natl. Acad. Sci. USA.*, 1998, **95**, 14821-14826.

20. dit Faute MA, Laurent L, Ploton D, Poupon MF, Jardillier JC, and Bobichon H., *Clin. Exp. Metastasis.*, 2002, **19**, 161-168.

21. Thomas Tyrel Goodman, Chee Ping Ng, and Suzie Hwang Pun, *Bioconjug. Chem.*, 2008, **19**, 1951-1959.

22. Vikash P. Chauhan, Triantafyllos Stylianopoulos, Yves Boucher, and Rakesh K. Jain, *Annu. Rev. Chem. Biomol. Eng.*, 2011, **2**, 281-298.

23. Sophia K Dean, Hayley Scott, Gregory W Keogh, Simon Roberts, and Bernard E Tuch, *Am. J. Vet. Res.*, 2002, **63**, 1501-1506.

24. Schultz GS, and Wysocki A., *Wound Repair Regen.*, 2009, 17, 153-162.

25. Emmanuel Farge, *Curr. Top. Dev. Biol.*, 2011, **95**, 243-265.

26. Michael S. Samuel, Jose I. Lopez, Ewan J. McGhee, Daniel R. Croft, David Strachan, Paul Timpson, June Munro, Ewald Schröder, Jing Zhou, Valerie G. Brunton, Nick Barker, Hans Clevers, Owen J. Sansom, Kurt I. Anderson, Valerie M. Weaver, and Michael F. Olson, *Cancer Cell.*, 2011, **19**, 776-791.

27. Paul A. Janmey, and R. Tyler Miller, *J. Cell Sci.*, 2011, **124**, 9-18.

28. Jonathan T Butcher, and Robert Nerem, *J. Heart Valve Dis.*, 2004, **13**, 478-485.

29. Kristyn S. Masters, Darshita N. Shah, Gennyne Walker, Leslie A. Leinwand, and Kristi S. Anseth, *J. Biomed. Mater. Res. A.*, 2004, **71**, 172-180.

30. Abdel Kareem Azab, Boris Orkin, , Victoria Doviner, Aviram Nissan, Martine Klein, Morris Srebnik, and Abraham Rubinstein, *J. Control Release.*, 2006, **111**, 281-289.

31. Sarmistha Talukdar, Mahitosh Mandal, Dietmar W. Hutmacher, Pamela J. Russell, Carolina Soekmadji, and Subhas C. Kundu, *Biomaterials.*, 2011, **32**, 2149-2159.

32. Venkat Chokkalingam, Jurjen Tel, Florian Wimmers, Xin Liu, Sergey Semenov, Julian Thiele, Carl G. Figdor, and Wilhelm T.S. Huck, *Lab Chip.*, 2013, **13**, 4740-4744.

33. Wilfried Weber, Matthias Rinderknecht, Marie Daoud-El Baba, François-Nicolas de Glutz, Dominique Aubel, and Martin Fussenegger, *J. Biotechnol.*, 2004, **114**, 315-326.

34. Otterlei M, Ostgaard K, Skjåk-Braek G, Smidsrød O, Soon-Shiong P, and Espevik T., *J. Immunother.*, 1991, **10**, 286-291.

35. Espevik T, Otterlei M, Skjåk-Braek G, Ryan L, Wright SD, and Sundan A., *Eur. J. Immunol*., 1993, **23**, 255-261.

36. Soon-Shiong P, Otterlie M, Skjak-Braek G, Smidsrod O, Heintz R, Lanza RP, and Espevik T., *Transplant Proc.*, 1991, **23**, 758-759.

37. Tan W, Krishnaraj R, and Desai TA, *Tissue Eng*., 2001, **7**, 203-210.

38. Dhananjay Dendukuri, Shelley S. Gu, Daniel C. Pregibon, T. Alan Hatton, and Patrick S. Doyle, *Lab Chip.*, 2007, **7**, 818-828.

39. Wayne R. Gombotz, Wang Guanghui, Thomas A. Horbett, and Allan S. Hoffman, *J. Biomed. Mater. Res.*, 1991, **25**, 1547-1562.

40. Daniela Loessner, Kathryn S. Stok, Matthias P. Lutolf, Dietmar W. Hutmacher, Judith A. Clements, and Simone C. Rizzi, *Biomaterials.*, 2010, **31**, 8494-8506.

41. Lin CC, and Anseth KS., *Proc. Natl. Acad. Sci. U S A.*, 2011, **108**, 6380-6385.

42. Su J, Hu BH, Lowe WL Jr, Kaufman DB, and Messersmith PB., *Biomaterials.* 2010, **31**, 308-314.

43. Otterlei M1, Ostgaard K, Skjåk-Braek G, Smidsrød O, Soon-Shiong P, and Espevik T., *J. Immunother.*, 1991, **10**, 286-291.

44. Espevik T, Otterlei M, Skjåk-Braek G, Ryan L, Wright SD, and Sundan A, *Eur. J. Immunol*., 1993, **23**, 255-261.

45. Soon-Shiong P, Otterlie M, Skjak-Braek G, Smidsrod O, Heintz R, Lanza RP, and Espevik T., *Transplant Proc.*, 1991, **23**, 758-759.

46. Tan W, Krishnaraj R, and Desai TA, *Tissue Eng*., 2001, **7**, 203-210.

47. Venkat Chokkalingam, Jurjen Tel, Florian Wimmers, Xin Liu, Sergey Semenov, Julian Thiele, Carl G. Figdor, and Wilhelm T.S. Huck, *Lab Chip.*, 2013, **13**, 4740-4744.

48. Hartgerink JD, Beniash E, and Stupp SI, *Science*., 201, **294**, 1684-1688.

49. Lin CC, and Anseth KS., *Proc. Natl. Acad. Sci. U S A.*, 2011, **108**, 6380-6385.

50. Su J, Hu BH, Lowe WL Jr, Kaufman DB, and Messersmith PB., *Biomaterials.*, 2010, **31**, 308-314.

51. Swaran JS Flora, *Oxid. Med. Cell Longev*., 2009, **2**, 191-206.

52. Barbara Brodsky, and Anton V. Persikov, *Adv. Protein. Chem.*, 2005, **70**, 301-339.

53. Varun Gauba, and Jeffrey D. Hartgerink, *J. Am. Chem. Soc.*, 2007, **129**, 2683-2690.

54. Raymond P. Boot-Handford, and Danny S. Tuckwell, *Bioessays.*, 2003, **25**, 142-151.

55. Johanna Myllyharju, and Kari I. Kivirikko, *Trends Genet.*, 2004, **20**, 33-43.

56. Sylvie Ricard-Blum, *Cold Spring Harb. Perspect. Biol.*, 2011, **3**, a004978.

57. Aron Parekh, and Alissa M Weaver, *Cell Adh. Migr.*, 2009, **3**, 288-292.

58. Fallica B, Maffei JS, Villa S, Makin G, and Zaman M, *PLoS One.*, 2012, **7**, e48024.

59. Deborah L Holliday, Kellie T Brouilette, Anja Markert, Linda A Gordon, and J Louise Jones, *Breast Cancer Res.*, 2009, **11**, R3.

60. Velazquez OC, Snyder R, Liu ZJ, Fairman RM, and Herlyn M, *FASEB J.*, 2002, **16**, 1316-1318.

61. Huang CP, Lu J, Seon H, Lee AP, Flanagan LA, Kim HY, Putnam AJ, and Jeon NL, *Lab Chip.*, 2009, **9**, 1740-1748.

62. Aron Parekh, and Alissa M Weaver, *Cell Adh. Migr.*, 2009, **3**, 288-292.

63. Vernella Vickerman, Jennifer Blundo, Seok Chung, and Roger Kamm, *Lab Chip.*, 2008, **8**, 1468-1477.

64. Suzan Commandeur, Vincent van Drongelen, Frank R. de Gruijl, and Abdoelwaheb El Ghalbzouri, *Cancer Sci*, 2012, **103**, 2120-2126.

65. Klar AS, Böttcher-Haberzeth S, Biedermann T, Schiestl C, Reichmann E, and Meuli M, *Pediatr. Surg. Int.*, 2014, **30**, 223-231.

66. Dhimolea E, Maffini MV, Soto AM, and Sonnenschein C, *Biomaterials.*, 2010, **31**, 3622-3630.

67. Katarina Wolf, Yi I. Wu, Yueying Liu, Jörg Geiger, Eric Tam, Christopher Overall, M. Sharon Stack, and Peter Friedl, *Nat. Cell Biol.*, 2007, **9**, 893-904.

68. Hsiao AY, Tung YC, Kuo CH, Mosadegh B, Bedenis R, Pienta KJ, and Takayama S, *Biomed. Microdevices.*, 2012, **14**, 313-323.

69. Tung YC1, Hsiao AY, Allen SG, Torisawa YS, Ho M, and Takayama S, *Analyst.*, 2011, **136**, 473-478.

70. Kunz-Schughart LA, Freyer JP, Hofstaedter F, and Ebner R, *J. Biomol. Screen.*, 2004, **9**, 273-285.

71. Hon Fai Chan, Ying Zhang, Yi-Ping Ho, Ya-Ling Chiu, Youngmee Jung, and Kam W. Leong, *Sci. Rep.*, 2013, **3**, 3462.

72. Feng Xu, BanuPriya Sridharan, ShuQi Wang, Umut Atakan Gurkan, Brian Syverud, and Utkan Demirci, *Biomicrofluidics.*, 2011, **5**, 022207.

73. Sungmin Hong, Hui-Ju Hsu, Roland Kaunas, and Jun Kameoka, *Lab Chip*., 2012, **12**, 3277-3280.

74. Dhananjay Denukuri, Daniel C. Pregibon, Jesse Collins, T. Alan Hatton, and Patrick S. Doyle, *Nature Materials*, 2006, **5**, 365-369.

75. Lee WR, Oh KT, Park SY, Yoo NY, Ahn YS, Lee DH, Youn YS, Lee DK, Cha KH, and Lee ES, *Colloids Surf. B Biointerfaces.*, 2011, **85**, 379-384.

76. Feng Xu, Jonathan Celli, Imran Rizvi, Sangjun Moon, Tayyaba Hasan, and Utkan Demirci, *Biotechnol. J.*, 2011, **6**, 204-212.

77. Boland T, Xu T, Damon B, and Cui X, *Biotechnol. J.*, 2006, **1**, 910-917.

78. Nakamura M, Kobayashi A, Takagi F, Watanabe A, Hiruma Y, Ohuchi K, Iwasaki Y, Horie M, Morita I, and Takatani S, *Tissue Eng.*, 2005, **11**, 1658-1666.

79. Odde DJ, and Renn MJ, *Trends Biotechnol.*, 1999, **17**, 385-389.

80. Guillaume Frasca, Florence Gazeau, and Claire Wilhelm, *Langmuir.*, 2009, **25**, 2348-2354.

81. Le Renard PE, Jordan O, Faes A, Petri-Fink A, Hofmann H, Rüfenacht D, Bosman F, Buchegger F, and Doelker E, *Biomaterials.*, 2010, **31**, 691-705.

82. Filip Ilievski, Aaron D. Mazzeo, Robert F. Shepherd, Xin Chen, and George M. Whitesides, *Angew. Chem. Int. Ed.*, 2011, **50**, 1890-1895.

83. Ruei-Zhen Lin, and Hwan-You Chang, *Biotechnol. J.*, 2008, **3**, 1172-1184.

84. Rasheena Edmondson, Jessica Jenkins Broglie, Audrey F. Adcock, and Liju Yang, *Assay Drug Dev. Technol.*, 2014, **12**, 207-218.

85. G. M. Whitesides, E. Ostuni, S. Takayama, X. Jiang, and D. E. Ingber, *Annu. Rev. Biomed. Eng.*, 2001, **3**, 335.

86. Andrew Rape. Wei-hui Guo, and Yu-li Wang, *J. Cell Science.*, 2011, **124**, 4233-4240.

87. Tana Y, Cristini V, and Lee A. P., *Sen. Actuators. B.*, 2006, **114**, 350.

88. Chen C, Abate A, Lee D, Eugene M, Terentjev M, and Weitz D, *Adv. Mater.*, 2009, **21**, 3201.

89. Yeh C, Zhao Q, Lee S, and Lin Y, *Sen. Actuators. A.*, 2009, **151**, 231.

90. Yu B, Cong H, Liu X, Ren Y, Wang J, Zhang L, Tang J, Ma Y, and Akasaka T, *J. Micromech. Microeng.*, 2013, **23**, 095016.

91. Hwang D, Dendukuri D, and Doyle P, *Lab Chip.*, 2008, **8**, 1640.

92. Xu S, Nie Z, Seo M, Lewis P, Kumacheva E, Stone H, Garstecki P, Weibel D, Gitlin I, and Whitesides G.M, *Angew. Chem. Int. Ed.*, 2005, **44**, 724.

93. Yung-Chieh Tana, Vittorio Cristini, and Abraham P. Lee, *Sen. Actuators. B.*, 2006, **114**, 350-356.

94. Liu SH, Yang RS, al-Shaikh R, and Lane JM, *Clin. Orthop. Relat. Res.*, 1995, **318**, 265-278.

95. H. Kang, K. J. Bayless, and R. Kaunas, *Am. J. Physiol.: Heart Circ. Physiol.*, 2008, **295**, H2087.

96. K. J. Bayless, and G. E. Davis, *Biochem. Biophys. Res. Commun.*, 2003, **312**, 903.

97. G. E. Davis, and C. W. Camarillo, *Exp. Cell Res.*, 1996, **224**, 39.

98. Ogden, R., and W. Large, *Proceedings of the Royal Society of London. Series A, Mathematical and Physical Sciences.*, 1972, **326**, 565-584.

99. Lan SF, and Starly B, *Toxicol. Appl. Pharmacol.*, 2011, **256**, 62-72.

100. Zehong Yang, and Xiaojun Zhao, *Int. J. Nanomedicine.*, 2011, **6,** 303-310.

101. Dhiman HK, Ray AR, and Panda AK, *Biomaterials.*, 2005, **26**, 979-986.

102. Bharadwaj, Rajnish, and Yu, Hongtao, *Oncogene.*, 2004, **23**, 2016-2027.

103. Brito, D. A., Yang, Z., and Rieder, C. L., *J. Cell Biol.*, 2008, **182**, 623-629.

104. M.A. Jordan, and L. Wilson, *Nat. Rev. Cancer.*, 2004, **4**, 253-265.

105. A. Ganguly, H. Yang, and F. Cabral, *Mol. Cancer Ther.*, 2010, **9**, 2914-2923.

106. J. Lowe, H. Li, K.H. Downing, and E. Nogales, *J. Mol. Biol.*, 2001, **313**, 1045-1057.

107. Colby AH, Colson YL, and Grinstaff MW, *Nanoscale.*, 2013, **5**, 3496-3504.

108. Nikki A. Evensen, Jian Li, Jie Yang, Xiaojun Yu, Nicole S. Sampson, Stanley Zucker, and Jian Cao, *PLoS One.*, 2013, **8**, e82811.

109. John A. Hickman, Ralph Graeser, Ronald de Hoogt, Suzana Vidic, Catarina Brito, and Matthias Gutekunst, *Biotechnol. J.*, 2014, **9**, 1115-1128.

110. Barcellos-Hoff MH, Aggeler J, Ram TG, and Bissell MJ, *Development.*, 1989, **105**, 223-235.

111. Xu HB, Hunag KX, and Zhu YS, *Pharmacol. Res.*, 2002, **46**, 459-467.

112. King MJ, Badea I, Solomon J, Kumar P, Gaspar KJ, and Foldvari M, *Diabetes Technol Ther.*, 2002, **4**, 479-488.

113. Iyer H, Khedkar A, and Verma M, *Diabetes Obes. Metab.*, 2010, **12**, 179-185.

114. Kalra S, Bharti K, and Agrawal N, *Diavetol Metab. Syndr.*, 2010, **8**, 66.

115. Decker E, Coimbra C, and Weekers L, *Transplant Proc.*, 2009, **41**, 3389-3392.

116. Desai TA, Chu WH, Tu JK, Beattiw GM, Hayek A, and Ferrari M., *Biotechnol. Bioeng*., 1998, **57**, 118-120.

117. Freitas RA Jr, *Stud. Health Technol. Inform.*, 2002, **80**, 45-49.

118. Meetoo D, *Br. J. Nurs*., 2004, **13**, 644-651.

119. Gates BD, Xu QB, Stewart M, Ryan D, Willson CG, and Whitesides GM. *Chemical Reviews.*, 2005, **105**, 1171.

120. Glangchai LC, Caldorera-Moore M, Shi L, and Roy K., *J. Control Release.*, 2008, **125**, 263-272.

121. Takei S, Ogawa T, Deschner R, Jen K, Nihira T, Hanabata M, and Willson CG, *Japanese Journal of Applied Physics*., 2010, **49**, 075201.

122. Matthew E. Helgeson, Stephen C. Chapin, and Patrick S. Doyle, *Curr. Opin. Colloid Interface Sci.*, 2011, **16**, 106.

123. Chong Qiu, Meisha Chen, Hui Yan, and Hongkai Wu, *Adv. Mater.*, 2007, **19**, 1603.

124. Dhananjay Dendukuri, Daniel C. Pregibon, Jesse Collins, T. Alan Hatton and Patrick S. Doyle, *Nature Material.*, 2006, **5**, 365.

125. Laney M. Weber, Kirsten N. Hayda, Kathryn Haskins, and Kristi S. Anseth, *Biomaterials.*, 2007, **28**, 3004-3011.

126. Chien-Chi Lin, and Kristi S. Anseth, *Proc. Natl. Acad. Sci. U S A.*, 2011, **108**, 6380-6385.

127. Dong Yang, and Kim S. Jones, *J. Biomed. Mater. Res. A.*, 2009, **90**, 411-418.

128. Elleri D, Dunger DB, and Hovorka R., *BMC Med*, 2011, **9**, 120.

129. A Ilieva, S Yuan, R N Wang, D Agapitos, and D J Hilland L Rosenberg, *J. Endocrinol.*, 1999, **161**, 357-364.

130. Alex Rabinovitch, and Wilma L. Suarez-Pinzon, *Biochem. Pharmacol.*, 1998, **55**, 1139-1149.

131. X. Lei, S. Zhang, B. Emani, S. E. Barbour, and S. Ramanadham, *Diabetes Obes. Metab.*, 2010, **12**, 93-98.

132. Natsuki Nagata , Asuka Iwanaga , Kazutomo Inoue, and Yasuhiko Tabata, *J. Biomater. Sci. Polym. Ed.*, 2002, **13**, 579-590.

133. Yung-Chieh Tana, Vittorio Cristini, and Abraham P. Lee, *Sen. Actuators. B.*, 2006, **114**, 350.

134. Chia-Hung Chen, Adam R. Abate, Daeyeon Lee, Eugene M. Terentjev, and David A. Weitz. *Adv. Mater.*, 2009, **21**, 3201.

135. Chia-Hsien Yeh, Qiaole Zhao, Sheng-Ji Lee, and Yu-Cheng Lin., *Sen. Actuators. A.*, 2009, **151**, 231.

136. Bing Yu, Hailin Cong, Xuesong Liu, Yumin Ren, Jilei Wang, Lixin Zhang, Jianguo Tang, Yurong Ma, and Takeshi Akasaka. *J. Micromech. Microeng.*, 2013, **23**, 095016.

137. Dae Kun Hwang, Dhananjay Dendukuri, and Patrick S. Doyle, *Lab Chip.*, 2008, **8**, 1640.

138. Shengqing Xu, Zhihong Nie, Minseok Seo, Patrick Lewis, Eugenia Kumacheva, Howard A. Stone, Piotr Garstecki, Douglas B. Weibel, Irina Gitlin, and George M. Whitesides, *Angew. Chem. Int. Ed.*, 2005, **44**, 724.

139. Sungmin Hong, Hui-Ju Hsu, Roland Kaunas, and Jun Kameoka, *Lab Chip.*, 2012, **12**, 3277.

140. Maynor BW, Larue I, Hu Z, Rolland JP, Pandya A, Fu Q, Liu J, Spontak RJ, Sheiko SS, Samulski, RJ, Samulski ET, and DeSimone JM, *Small*, 2007, **3**, 845.

141. Rolland JP, Maynor BW, Euliss LE, Exner AE, Denison GM, and DeSimone JM, *J. Am. Chem. Soc.*, 2005, **127**, 10096.

142. Acharya G, Shin CS, McDermott M, Mishra H, Park H, Kwon IC, and Park K., *J Control Release.*, 2010, **141**, 314-319.

143. Alison P. McGuigan, Derek A. Bruzewicz, Ana Glavan, Manish Butte, and George M. Whitesides, *PLoS One.*, 2008, **3**, e2258.

144. H. Kang, K. J. Bayless, and R. Kaunas, *Am. J. Physiol.: Heart Circ. Physiol.*, 2008, **295**, H2087.

145. Samarasinghe SAPL, Shao Y, Huang P-J,Pishko M, Chu K-H, and Kameoka J, *PLoS One.*, 2016, **11**, e0165839.

146. Laney M. Weber, Kirsten N. Hayda, and Kristi S. Anseth, *Tissue Engineering Part A.*, 2008, **14**, 1959-1968.

147. Yoon JW, and Jun HS, *Am. J. Ther.*, 2005, **12**, 580-591.

148. Yasutaka Fujita, Morihito Takita, Masayuki Shimoda, Takeshi Itoh, Koji Sugimoto, Hirofumi Noguchi, Bashoo Naziruddin, Marlon F. Levy, and Shinichi Matsumoto, *Islets.*, 2011, **3**, 1-5.

149. Laney M. Weber, Kirsten N. Hayda, and Kristi S. Anseth, *Tissue Engineering A.*, 2008, **14**, 1959-1968.

150. Shapiro AM, Lakey JR, Ryan EA, Korbutt GS, Toth E, Warnock GL, Kneteman NM, and Rajotte RV, *N Engl J Med.*, 2000, **343**, 230-238.

151. Naoaki Sakata, Shoichiro Sumi, Gumpei Yoshimatsu, Masafumi Goto, Shinichi Egawa, and Michiaki Unno, *World J Gastrointest Pathophysiol.*, 2012, **3**, 19-26.

152. Drachenberg CB, Klassen DK, Weir MR, Wiland A, Fink JC, Bartlett ST, Cangro CB, Blahut S, and Papadimitriou JC, *Transplantation.*, 1999, **68**, 396-402.

153. Tanemura M, Saga A, Kawamoto K, Machida T, Deguchi T, Nishida T, Sawa Y, Doki Y, Mori M, and Ito T, *Transplant Proc.*, 2009, **41**, 334-338.

154. Qi M, Gu Y, Sakata N, Kim D, Shirouzu Y, Yamamoto C, Hiura A, Sumi S, and Inoue K, *Biomaterials.*, 2004, **25**, 5885-5892.

155. Murua A, Portero A, Orive G, Hernández RM, de Castro M, and Pedraz JL, *J Control Release.*, 2008, **132**, 76-83.

156. A P Monaco, T Maki, H Ozato, M Carretta, S J Sullivan, K M Borland, M D Mahoney, W L Chick, T E Muller, and J Wolfrum, *Ann. Surg.*, 1991, **214**, 339-362.

157. Johansson H, Goto M, Dufrane D, Siegbahn A, Elgue G, Gianello P, Korsgren O, and Nilsson B, *Am. J. Transplant.*, 2006, **6**, 305-312.

158. Sakata N, Obenaus A, Chan N, Mace J, Chinnock R, and Hathout E, *Islets.*, 2009, **1**, 26-23.